Analysis of FRP shear strengthening solutions for reinforced concrete beams considering debonding failure

Denise Ferreira[1], Eva Oller[2], Antonio Marí[3], Jesús Bairán[4]

Corresponding autor: Eva Oller, eva.oller@upc.edu

Abstract

In this paper, a fiber beam model previously developed by the authors for the nonlinear analysis of strengthened elements, including the effects of shear, is used to predict the response of reinforced concrete (RC) beams strengthened in shear with fiber reinforced polymers (FRP) sheets. In the previous version of the model, debonding failure of FRP was not included; hence, its application was limited to the simulation of wrapped configurations. The model is now extended to account for debonding failure in order to allow for its application to beams strengthened with U-shaped and side-bonded configurations. Existing experimental tests on RC beams strengthened in shear by FRP sheets in both wrapped and U-shaped configurations were numerically simulated. The model reproduces, with reasonable accuracy, the experimental failure loads, the load-deflection behavior and the strains in FRP and stirrups with increasing load. The advantages of this proposal are related with the simplicity and straightforwardness of the beam models to be applied in practical engineering problems.

Keywords: Strengthening, Shear, FRP laminates, debonding, fiber beam model

[1] Post-doc researcher, Civil and Environmental Engineering Department, Universitat Politècnica de Catalunya, Jordi Girona 1-3, C-1 201, 08034 Barcelona (Spain), denise.carina.santos@upc.edu

[2] Asssistant Professor, Civil and Environmental Engineering Department, Universitat Politècnica de Catalunya, Jordi Girona 1-3, C-1 201, 08034 Barcelona (Spain), eva.oller@upc.edu

[3] Professor, Civil and Environmental Engineering Department, Universitat Politècnica de Catalunya, Jordi Girona 1-3, C-1 201, 08034 Barcelona (Spain), antonio.mari@upc.edu

[4] Associate Professor, Civil and Environmental Engineering Department, Universitat Politècnica de Catalunya, Jordi Girona 1-3, C-1 201, 08034 Barcelona (Spain), jesus.miguel.bairan@upc.edu

INTRODUCTION

There is a lack of worldwide consensus on the evaluation of the contribution of the externally bonded (EB) FRP reinforcement to the shear strength, in elements strengthened in shear through this technique (Sas et al. 2009, Pellegrino et al. 2013). One of the main reasons for this might be the complexity of the resisting mechanisms, not only for the shear strengthening system but also for reinforced concrete. Another reason might be the difficult evaluation of the laminate debonding mechanisms, which can be related to the anchorage length of the FRP laminate once the critical shear crack opens.

The existing guidelines (ACI440.2R-08 2008, CNR-DT-200/2004 2004, Concrete Society TR-55 2012, fib Bulletin 14 2001, DAfStb Heft 595 2013) add the contribution of the EB FRP reinforcement to the shear strength of the unstrengthened element. However, changes in the strut orientation or additional cracking may change the contribution of the concrete or of the existing transverse reinforcement to the overall shear strength. The interaction of the FRP shear reinforcement with the transversal steel or the concrete is considered in some models based on plasticity (Colajani et al. 2005). In addition, a few number of existing formulations consider not only the interaction but also the laminate debonding (Modifi and Chaallal 2013, Monti and Liotta 2007, Kotynia 2011).

The FRP shear strengthening can be performed in different configurations: a) sheets fully wrapping the cross-section (wrapped); b) sheets or L-shaped laminates bonded on the lateral sides and the bottom surface of the beam (U-shaped); and c) sheets or laminates bonded in the lateral sides of the cross-section (side-bonded). The sheets and laminates can be bonded in a continuous or discontinuous configuration.

In the case of U-shaped or side-bonded configurations, the FRP may debond before reaching its ultimate capacity. Then, the ductility of beams failing in this mode is usually limited (Chen and Teng 2003). To avoid or delay this type of failure, some anchorage devices can be applied (Khalifa and Nanni 2000). These anchorage devices may consist of rods mounted on the web-flange corner to anchor the end of the FRP to the compression zone or may consist of steel profiles. However, the use of bolts or fasteners involves some inconveniences. The anchorage might damage the FRP fibers

during installation due to the execution of holes to the FRP, and some stress concentration can appear at the location of the fasteners (Mofidi et al. 2013).

This paper presents numerical studies on the effects of the FRP on the shear strength of RC beams and the mechanism of debonding failure for U-shaped or side-bonded configurations. A fiber beam model developed by the authors for the nonlinear analysis of RC and strengthened elements including the effects of shear (Ferreira et al. 2014a, 2014b, 2013a) is improved to account for debonding failure of FRP. It is then used to predict the response of RC beams strengthened in shear with FRP sheets in wrapped and U-shaped configurations. The model is validated through the analysis of some existing experimental campaigns (Alzate 2012, Mathhys 2000, Khalifa and Nanni 2002) on RC beams strengthened in shear with FRP sheets involving different configurations. An earlier version of the model, disregarding the debonding failure mechanism of FRP, was previously validated for the wrapped configuration (Ferreira et al. 2013b).The current model is validated by comparing the numerical results to those obtained in the experimental program. The model reproduces, with good accuracy, the experimental failure loads, the load-deflection behavior and the strains in stirrups and FRP with increasing load until failure. It also reflects the load-sharing between inner transversal steel reinforcement and EB FRP before and after premature debonding failure.

The original contribution of the present work is the consideration of debonding failure mechanism of FRP in a FEM based on fiber beam approach. This achievement is important due to its simplicity and computational speed to be applied at true scale structural analysis, making it an attractive tool for practical engineering.

DEBONDING FAILURE CRITERIA OF FRP IN SHEAR STRENGTHENING

As previously mentioned, U-shaped and side-bonded configurations of FRP usually fail due to debonding after the formation of a critical shear crack (Pellegrino and Modena, 2006). Therefore, a debonding criteria has to be considered in the numerical model in order to account for this type of failure. In flexural strengthening, the debonding failure can initiate either at intermediate cracks due to shear stresses (intermediate crack (IC) debonding), or near the end of the laminate (plate end (PE) debonding). When debonding occurs, the laminate does not contribute anymore to the cross-section strength, generally driving to the structural failure, as no equilibrium can be reached between applied

forces, reactions and internal forces. For shear strengthening, the debonding failure initiates once the shear critical crack opens. Then, the laminate debonds if the FRP bonded length from the shear crack to the laminate end is not enough to anchor or transfer the tensile force acting on the FRP. In the side-bonded case, debonding can be observed at both sides of the critical shear crack. In the U-shaped case, debonding occurs in the upper side of the shear crack.

The debonding failure approach implemented in the present model is that proposed by Oller et al. (2009). This formulation was originally developed for flexural strengthening to capture IC debonding failure and PE debonding. To predict debonding for FRP shear strengthening, the same formulation of the plate end debonding can be applied, assuming that for each strip the bonded length (L_b) is the FRP laminate length shown in Fig. 1. For U-shaped configurations, the bonded length of each strip is the bonded length above the critical shear crack. For side-bonded configurations, the bonded length of each strip is the minimum length of the laminate above or below the critical shear crack.

According to Oller et al. (2009), the maximum transferred force $F_{\max}$ along the bonded length L_b, can be expressed as:

$$F_{\max,Lb} = F_0 \begin{cases} \sin\left(\frac{\pi}{2}\frac{L}{L_{\lim}}\right) & L_b \le L_{\lim} \\ 1 & L_b > L_{\lim} \end{cases} \tag{1}$$

$$F_0 = b_L\sqrt{2G_F E_L t_L} \tag{2}$$

$$L_{\lim} = \frac{\pi}{2}\frac{\sqrt{2G_F E_L t_L}}{\tau_{LM}} \tag{3}$$

where: b_L = FRP width; t_L = FRP thickness; E_L = laminate modulus of elasticity; τ_{LM} = maximum shear stress at the interface given by Eq. (4); G_F = fracture energy or energy by unit area necessary to separate the laminate from the support given by Eq. (5). Units are in N and mm

$$\tau_{LM} = C_{\tau LM}\left(\frac{1}{f_{ctm}} + \frac{1}{f_{cm}}\right)^{-1} \tag{4}$$

$$G_F = C_{\tau LM}^2 C_F f_{ctm} \tag{5}$$

where f_{cm} = mean value of concrete compressive strength; f_{ctm} = mean value of concrete tensile

strength; $C\tau_{LM}$ = constant that ranges between 0.37 and 1.56 with a mean value of 0.87 and a standard deviation of 0.17 according to the shear test database assembled by Oller (2005); C_F = constant found to obtain the smallest standard deviation when predicting the experimental maximum force in a single or double shear test. For the shear test database compiled by Oller (2005), C_F varies between 0.15 and 0.62, with a mean value of 0.35 and a standard deviation of 0.07.

FIBER BEAM MODEL

Fundamentals of the model

The beam model with axial force – shear – bending interaction (*N-V-M*) uses a displacement-based FE formulation for the nonlinear phased analysis of concrete frame structures. The detailed formulation and validation of the 1D model with shear critical benchmarks was presented elsewhere (Ferreira et al. 2014a, 2014b, 2013a). Only a brief description of the fundamentals of the model is presented here.

Fig. 2 presents the general characteristics of the model for the different levels of analysis: element, section, fiber and material. Regarding the element level, the model is based on the Timoshenko beam theory with the cross-section discretized into fibers, the longitudinal reinforcement simulated by means of filaments and transversal reinforcement considered smeared in concrete. At the sectional level, a shear-sensitive model accounts for the nonlinear force interaction (*N-V-M*). The plane-section theory, that allows determining the longitudinal strains at each fiber as a function of the generalized strains of the section, is coupled with a constant shear stress constraint along the cross-section. Filaments of longitudinal reinforcement are only submitted to axial strains and stresses, following the plane section theory. Transverse reinforcement (internal steel stirrups and/or EB FRP) is accounted through its volumetric ratio ρ_{st} and is submitted to axial stresses σ_z^{st}. Compatibility requirements impose that the vertical strain ε_z in concrete is equal to the strain in the transverse reinforcement. The computed shear stresses τ_{xz} must equate the imposed shear stresses given by the fixed stress constraint τ^* of the sectional hypothesis. By guaranteeing these two requirements, the vertical axial strain ε_z and shear strain γ_{xz} of each fiber are outputted. This determination is not linear and an iterative procedure within the fiber level is needed.

Pertaining to the material simulation, a smeared and rotating crack approach is considered for concrete. The Hognestad parabola is considered for concrete in compression. Lateral effects of softening (Vecchio and Collins 1986) and strength enhancement (Kupfer et al. 1969) factors are included. When FRP strengthening is placed by means of a wrapped configuration, the increment of both peak strength and ultimate strain of concrete due to the confinement action is considered through the model of Spoelstra and Monti (1999). A linear response is assumed for uncracked concrete in tension and a tension stiffening curve (Cervenka 1985) is considered for the remaining stresses in the cracked stage. Longitudinal and transverse reinforcements (steel and FRP) are under 1D stress-strain states determined through linear uniaxial constitutive equations, with kinematic hardening for steel.

This model was previously applied to study FRP shear strengthened beams with wrapped configurations (Ferreira et al. 2013b). As explained in continuation, this model is extended to account for FRP debonding in shear (following the previously presented criteria of Oller et al. 2009) in order to expand its application to U-shaped and side-bonded configurations.

Debonding failure of FRP

Fig. 3 summarizes the input hypothesis considered in the sectional model, the output results and the criteria for checking FRP debonding failure. The gradients of vertical stresses between the border and the shear critical fiber are computed to be compared with the maximum transfer force. The shear critical fiber is considered to be located at $3/4 \cdot h$ (h in the total height of the cross section), being the critical tensile stress $\sigma_z^{FRP}(z = 3/4 \cdot h)$. This criteria is a consequence of the basic hypothesis of the model, resulting into higher shear strains and higher vertical strains in the more cracked areas (Ferreira 2013). Since the vertical stress in the border is null, the gradient is equal to the tensile stress in the critical fiber. The critical stress in the FRP, $\sigma_z^{FRP}(z = 3/4 \cdot h)$, is compared with the maximum vertical stress that can be transferred to the FRP, $\sigma_{max,deb}$, that corresponds to the maximum transferred force $F_{max,Lb}$ (Eq. 6).

$$\sigma_{\max,\mathrm{deb}} = \frac{F_{\max,Lb}}{b_L t_L} \tag{6}$$

When the stresses σ_z^{FRP} in the FRP laminate in the critical fiber reach the maximum allowed stress that can be transferred by bonding mechanism, the area of the FRP reinforcement of that cross-section

147 is set to zero, and the analysis may continue with redistribution of forces in the remaining steel stirrups
148 and FRP sheets in other cross sections. The tensional scheme in a fiber for the checking of bond
149 failure is represented in Fig. 4.

150 **VALIDATION OF THE MODEL**

151 **Experimental tests by Alzate (2012)**

152 An experimental program on FRP-shear strengthened RC beams was carried out by Alzate (2012)
153 with the purpose of studying the contribution of FRP to the shear resistance of RC elements. The
154 beams were simply supported, 4.5 m long and with a rectangular cross section of 0.42 m height and
155 0.25 m width. A RC beam critical to shear (control beam) was strengthened with different solutions of
156 FRP in terms of configuration and quantity and tested until failure. From the set of beams tested in the
157 experimental campaign, the beams strengthened in shear with vertical FRP strips were simulated. Each
158 beam was submitted to two load tests with different total spans and equal shear spans; only the long
159 total span configuration was simulated, with a concentrated load applied at a distance of 3 times the
160 total depth ($a = 3h = 1.26$ m) from the support. Geometry, internal reinforcement and strengthening
161 configurations of the specimens are represented in Fig. 5.

162 The beams are reinforced with FRP sheets of 300 mm of width presenting two different
163 thicknesses - S530 represent unidirectional fibers (530 g/m^2) with dry fiber thicknesses of 0.293 mm
164 and S330 represent unidirectional fibers (300 g/m^2) with dry fiber thicknesses of 0.176 mm - and two
165 different configurations - wrapped and U-shaped. The names of the tested specimens mean the
166 following: W90S530 is the beam with wrapped S530 FRP; U90S530 is the beam with U-shaped S530
167 FRP; W90S300 is the beam with wrapped S300 FRP; and U90S300 is the beam with U-shaped S300
168 FRP. The fibers of the FRP sheets formed an angle of 90º with respect to the longitudinal axis and the
169 sheets were spaced at 200 mm from edge to edge.

170 The beams with wrapped FRP strengthening present a ductile shear-bending related failure with
171 FRP rupture and crushing of concrete near the load application point; in contrast, the beams with U-
172 shaped configuration presented a brittle shear failure mechanism after FRP debonding (Fig. 6). No
173 reference to yielding of longitudinal reinforcement is made; however, the load-displacement curve of
174 the wrapped beams presents a plateau of displacements at peak load (demonstrating the ductility of the

response) which is not observed in the case of the U-shaped beams.

Experimental data available in Alzate (2012) includes vertical displacements at mid-span measured by displacement transducers and vertical strains in stirrups and in the FRP sheets monitored at the shear-span by means of bonded strain gages. The location of the sensors considered in the validation is represented in Fig. 5.

Numerical modelling

The FE mesh used in the numerical simulation is represented in Fig. 7: beam elements with 0.1 m length, cross-section discretized into fibers of 0.005 m height, longitudinal reinforcement simulated with steel filaments, both the transversal steel and FRP reinforcement considered smeared with their respective quantities and material properties. Different specimens of each type were tested (identified with –a, –b or –c) and also simulated; the only difference between them is the compression strength of concrete f_{cm}.

The material properties of concrete and FRP considered in the model are listed in Table 1. The concrete compression strength f_{cm} was measured in concrete specimens in the lab and is available in Alzate (2012). The remaining properties were determined by the equations of EC2 (2004), as function of the experimental value of f_{cm} (see Fig. 2 for the meanings of the material properties) (see Eqs. (7) to (9)). For the wrapped configurations, the confinement effect was considered, enhancing the mechanical properties of concrete. For the U-shaped configuration, confinement effect was neglected. For the beam with U-shaped configuration (U90), the parameters related to the debonding failure criteria (τ_{LM}, G_F and t_L) were determined as function of f_{cm} as shown in Table 1. The characteristics of the FRP are also listed in Table 1. For steel reinforcement, longitudinal and transversal, the following properties were considered: E_s = 200000 MPa, f_{sy} = 500, f_{su} = 580 MPa, ε_{su} = 0.10. Load was applied incrementally until failure.

$$f_{ctm} = 0.30 \cdot \sqrt[3]{f_{ck}^2} \quad if \ f_{ck} \le 60\, N/mm^2 \tag{7}$$

$$f_{ctm} = 2.12 \cdot \ln\left(1 + \frac{f_{cm}}{10}\right) \quad if \ f_{ck} > 60\, N/mm^2 \tag{8}$$

$$E_c = 22 \cdot \left(\frac{f_{cm}}{10} \right)^{0.3} \quad (9)$$

Results and discussion

The experimental and numerical shear force vs. deflection at mid span are compared in Fig. 8 for the two beams with different FRP configurations, wrapped (W90) and U-shaped (U90) and for the two series (S5 means series S530 and S3 means series S300); in case of existence of more than one specimen of each type they are identified with the letters -a, -b and -c).

The numerical results show a good agreement with the experimental response in terms of ultimate load and along the nonlinear path with increasing load. The summary of computed results at failure and the comparison with experimental data are presented in Table 2. From the graphics and the table it is observed that the model is able to predict a correct failure load of the beams with U-shaped FRP configurations because it accounts for debonding failure. In fact, the W- and U-shaped beams of each series have exactly the same geometry, reinforcement and quantity of stirrups and FRP; the only difference is the strengthening configuration. Laminate debonding failure in the U-shaped beam occurs before FRP reaches its maximum strength; as can be seen in the values of σ_z^{FRP} for the debonding instant in Table 2. When this value exceeds the maximum stress allowed to be transferred, $\sigma_{max,deb}$, the debonding mechanism occurs, setting the FRP area of the cross section to zero. From this point forward, this FRP element ceases its contribution to the structural response. For all the U-shaped strengthened beams, the model predicts failure right after debonding occurs, being not able to redistribute the forces; this is consistent with the experimental observations (Alzate 2012). The beams with the wrapped configurations fail when FRP reaches the ultimate capacity; hence presenting higher ultimate load carrying capacities, which is correctly captured by the model.

Only converged values are represented in the graphs. The last load step represented related to the last converged; the next one is when materials failure occurs. The analysis is not able to reach convergence in the last load step due to vast damage of materials.

The computed strains in the transversal reinforcement (inner steel stirrups and EB FRP) with increasing shear force are compared with the experimental measurements for the beams with different FRP strengthening configurations (Wrapped and U-shaped). Fig. 9 presents the results of series S530

and Fig. 10 of series S300; for location of the sensors see Fig. 5. Only one specimen of each type is represented; the other specimens presented similar fittings.

Despite the difficulty of this comparison, due to the discrete form of the real cracks and the assumption of smeared cracking by the model, a good consistency between numerical and experimental results can be observed. The load level for which the stirrups and the FRP reinforcement start to carry load is well captured by the model. This load level corresponds to the outset of diagonal cracking. Sensors 1 and 5 located in the bottom of the beam can be more influenced by bending cracking, and hence, of more difficult comparison. However, in general, it can be observed that the model is able to capture the overall response of the transverse reinforcement. The load sharing between external FRP and inner steel stirrups is discussed in detail in the following section.

Load sharing between external FRP and internal steel stirrups

The computed stresses in the transversal reinforcement (stirrups and FRP) are compared in Fig. 11 for the wrapped and U-shaped configurations; these results are related to the mid-height of the cross section at the mid shear span. In Fig. 11b it can be observed the load level for which FRP debonding occurs in the U-shaped beam and the drop of stresses in FRP for onward load levels. After the occurrence of debonding failure, shear stresses are transferred for the steel stirrups that where already yielded at this stage leading to its failure and consequent failure of the beam in shear. For the wrapped configuration (Fig. 11a), the FRP sheets continue to carry load until failure of the FRP; i.e., the load carrying capacity of the FRP is not limited by the loss of bond. In these graphs, the yielding of stirrups instant is also marked; it can be noticed that, before this point, FRP and steel stresses are similar; after yielding, steel cannot increase the load carrying capacity and hence, the FRP increases their stresses significantly. This is observed in both cases, in wrapped and U-shaped configurations.

The computed strains and stresses of the transverse reinforcement (inner steel stirrups and EB FRP) throughout the cross section located at the mid shear span of the beams with U-shaped configuration are presented in Figs. 12 and 13, respectively, for the load levels near start of yielding of transversal steel reinforcement. Bond-slip is not directly considered in the numerical model (only the debonding failure is considered) resulting into equal strains computed in the vertical direction in the FRP and steel stirrups. For this reason only one graph is presented in Fig. 12 for each series (S530 and

S300).

Fig. 13 presents the stresses in the stirrups and in the FRP separately for each series (S530 and S300). The results correspond to the specimens U90S530-a and U90S300-b.

The strains (Fig. 12) and stresses (Fig. 13) presented in these graphs correspond to three load levels: immediately before yielding, yielding of transversal steel reinforcement located in the shear critical fiber (located at mid-shear span at 3/4h) and immediately after yielding. It can be observed that, yielding of steel reinforcement is spreading from the bottom to the top of the cross section. When yielding of transversal reinforcement is reached in a fiber, the strains and stresses increase in the FRP in order to compensate the fact that steel entered in the plastic phase. This can be seen in the change of the inclination of the diagrams of strains and stresses in FRP in the location of the yielded fiber.

The same presentation of results, strains (Fig. 14) and stresses (Fig. 15) along the shear critical cross section, is performed for the load levels near debonding of FRP. Respectively, the strains and stresses presented in these graphics correspond to three load levels: immediately before debonding, at debonding and immediately afterwards. It can be observed how the strains increase significantly when debonding occurs (Fig. 14a and 14b); and how the FRP ceases to contribute to shear resistance mechanism at the moment and after occurrence of peeling (Fig. 15b). For this stage of advanced loading and damage, stirrups are yielded in a large portion of the height of the cross section, as can be observed in Fig. 15a, and hence, are not capable of increasing stresses, only strains. It can be observed, that after debonding, the yielding of the stirrups propagates to the top fibers; however, this transference is very limited, as it immediately reaches the neutral axis. As the stirrups are already extensively yielded in the moment of FRP debonding, is not possible to transfer the forces carried out by the FRP to the transversal steel, and consequently, failure occurs right afterwards.

Experimental tests by Matthys (2000)

The experimental campaign carried out by Matthys (2000) consisted on RC beams strengthened in shear by means of different configurations of externally bonded FRP reinforcement. The beams were simply supported, with 4.0 m long and with a rectangular cross section of 0.45 m height and 0.2 m width, tested under 4-point loading until failure. From the 5 beams tested with different types of FRP reinforcement, two were considered for simulation in this work, corresponding to the U-shaped

280 configuration: BS4 (continuous FRP) and BS5 (3 discontinuous strips of FRP in each shear span).
281 Thickness and properties of the FRP are the same for both specimens; the amount of longitudinal
282 reinforcement (6 rebars of 20 mm of diameter) and inner transversal reinforcement (stirrups of 6 mm
283 of diameter spaced of 400 mm) are also equal. Experimental data available consists on curves of load
284 vs. displacements and strains in FRP in different positions in the beams. The geometry and positions
285 of the strain gauges are represented in Fig. 16.

286 Due to the different ratios of FRP reinforcement, these two beams presented different behaviors:
287 BS4 presented a ductile response in failure with crushing of concrete in the mid-spam and yielding of
288 longitudinal reinforcement; and BS5 presented a brittle shear failure with FRP rupture and subsequent
289 debonding.

290 ***Numerical modelling***

291 The FE mesh used is presented in Fig. 17, with beam elements of 0.1 m length, cross section
292 discretized into 0.01 m height, longitudinal reinforcement simulated with steel filaments, transverse
293 reinforcement (steel and FRP) as smeared. The material properties of concrete and FRP, and the
294 debonding failure criteria parameters are included in Table 1, corresponding to the experimental lab
295 tests reported in Matthys (2000). No confinement effect was considered due to the FRP. The following
296 properties were considered for steel (as reported in Mattys 2000): for rebars with 20 mm of diameter
297 (longitudinal reinforcement) E_s = 200000 MPa, f_{sy} = 530 MPa, f_{su} = 620 MPa, ε_{su} = 0.119; for rebars
298 with 6 mm of diameter (stirrups) E_s = 200000 MPa, f_{sy} = 560 MPa, f_{su} = 590 MPa, ε_{su} = 0.051.

299 ***Results and discussion***

300 The experimental curves of load vs. displacements are compared with the computed results in Fig.
301 18 for the two tests. The different ductility on the behavior of these two specimens under increasing
302 load can be observed: BS4 was not limited by a reduced shear capacity and reached its bending
303 capacity, probably due to the higher amount of FRP (continuous along the shear span; in contrast,
304 BS5, with less amount of FRP (discontinuous strips along the shear span) presented a shear failure
305 with rupture and debonding of FRP at a lower load level. The numerical model is consistent with the
306 experimental response under increase loading and with the observed failure mechanisms. A summary
307 of results at failure is included in Table 2.

The vertical strains measured in the FRP at different points of the shear span are compared in Fig. 19 with the results of the numerical model, for both specimens. Both graphs present the same scales to show the small strains observed in BS4, less sensitive to shear and without relevant diagonal cracking, when compared with BS5, which is a shear critical beam, developing important strains in FRP for higher load levels. It is observed that for the peak load in BS5, FRP strains were near the ultimate value; and the tensile stresses are far from the maximum debonding limit (see Table 2).

Experimental tests by Khalifa and Nanni (2002)

Khalifa and Nanni (2002) performed an experimental program of beams with (SW type) and without (SO type) stirrups strengthened in shear by continuous or discontinuous CFRP U-shaped sheets with one (90º) or two plies (0-90º). The beams had a rectangular cross section of 150 mm wide and 305 mm deep. All beams were tested under 4-point loading until failure with different shear spans. Two different a/d relationships were tested: 3 and 4. Five beams (SO-3-2, SO-3-3, SO-3-4, SO-4-2 and SO-4-3) were considered for simulation in this work. Four 32 mm diameter rebars were used as longitudinal reinforcement with (two at top and two at bottom face of the cross-section). In series SO, no stirrups were provided in one side of the beam. Experimental data available consists on curves of load vs. displacements and strains in FRP for beam SO-3-4. The geometry and positions of the strain gauges are represented in Fig. 20.

All analyzed beams failed due to laminate debonding except for beam SO-4-3 that failed due to concrete splitting.

Numerical modelling

The FE mesh used beam elements with 0.1 m of length, cross section discretized into 0.01 m height, longitudinal reinforcement simulated with steel filaments, transversal reinforcement (steel and FRP) as smeared. The material properties of concrete and FRP are included in Table 1. No confinement effect was considered. The following properties were considered for steel (Khalifa and Nanni, 2002): E_s = 200000 MPa, f_{sy} = 460 MPa, f_{su} = 7300 MPa.

Results and discussion

Fig. 21 shows the comparison between experimental and numerical results in terms of load vs. displacements. A good correlation is observed in general, in terms of ultimate load and overall

response under increasing loading. A summary of results at failure is included in Table 2. Ultimate load is overestimated by the numerical model for beam SO-3-4, which can be due to uncertainties on the properties related to bonding resistance. For all the other beams, the predicted ultimate load is similar to the experimental values.

Since these specimens had no internal transversal steel reinforcement in the critical shear span, the FRP debonding leads to an immediate loss of equilibrium of internal forces and failure. That is the reason why the predicted shear load for start of debonding is equal to the ultimate shear load for some of the beams (SO-3-2, SO-4-2). For the other specimens (SO-3-3, SO3-4, SO-4-3) the model predicted shear failure previously to debonding of FRP.

Fig. 22 compares the FRP strains at different locations along the SO-4-2 beam. The experimental results show that the FRP strain was zero prior to diagonal crack formation (around 80kN of shear force) increasing significantly until failure. The maximum local CFRP vertical strain measured at failure was approximately 0.0045. Given the difficulties on comparing experimental results and predictions based on smeared cracked approaches, the numerical results fit reasonably within the range of the experimental values, being able to capture the start of loading of FRP reinforcement and strain level in failure.

Comparison of the numerical FRP stresses at debonding to the guidelines predictions

Table 3 shows the numerical values of the FRP stresses at debonding stage which are compared to the values given by the existing design guidelines (Fib Bulletin 14 2001, ACI-440.2R-08 2008, CNR-DT200/2004, TR-55 2012, DafStb Heft 595 2013) to obtain the FRP shear strength contribution. In addition, it presents the ratio between the numerical and analytical values in brackets. As observed, the predictions of the Fib Bulletin are closest to the numerical values, although in some cases it overestimates the FRP stresses. The remaining guidelines are more conservative, underestimating the stresses in the external reinforcement. For instance, the mean ratio between the numerical and the analytical predictions for all tests of Alzate (2012) are: 0.97 for the Fib Bulletin 14, 1.56 for the ACI-440.2R-08, 1.67 for the CNR-DT-200/2004, 1.32 for the TR-55 and 1.36 for the DafStb Heft 595.

Study of the efficiency of FRP strengthening system to increase the shear capacity

This part of the paper aims to demonstrate how the model can be used as a tool for studying the

efficiency of FRP strengthening solutions for beams critical to shear.

The model was already extensively validated for the cases of shear critical RC beams (Ferreira et al. 2014a, 2014b, 2013a). As an example, the shear critical RC beam taken as the control specimen of Alzate's experimental campaign is correctly simulated by the model as can be observed in Fig. 23. The model captures the shear failure mode of the beam as explained in Ferreira et al. (2013b).

The model can be used to predict the gain of shear resistance brought by different strengthening solutions, as exemplified with the U-shaped and wrapped configurations with S530 and S300 FRP sheets used in the Alzate's (2012) experimental work. Fig. 24 presents the increment of load carrying capacity brought by the different solutions of FRP strengthening in shear. The strengthening interventions lead to, not only an increase of shear capacity and consequent load carrying capacity, but also, an increase of ductility. It also attained a change in the failure mode from brittle shear to bending with plasticity of the longitudinal reinforcement and ductile response.

These results demonstrate how the model can be used to assess the load carrying capacity of RC beams critical to shear and to predict the gaining of shear resistance achieved from different solutions of FRP strengthening in terms of shape and quantity. This can lead to a more efficient and rational design of the strengthening measure.

CONCLUSIONS

Debonding failure of FRP in shear strengthened RC beams is studied in this paper by means of a numerical model based on the fiber beam aproach. The previous version of this model was limited to the application of wrapped configurations as it disregarded this premature type of failure FRP. This paper describes the enhancement of the model to account for FRP debonding extending its use to sided and U-shaped configurations of externally bonded reinforcement. Experimental tests available in literature were numerically simulated. From these analyses the following conclusions are drawn:

- The model is able to correctly capture the load-displacement response of the strengthened beams with wrapped and U-shaped configurations;
- The model captured the overall response of the transverse reinforcement (inner steel stirrups and EB FRP), capturing the debonding of FRP and subsequent failure of the beams for the U-shaped configurations;

- When debonding failure occurs and FRP ceases its contribution to the shear resistance, stirrups were already extensively yielded and were no longer able to absorb the redistribution of forces, and failure occurred right after.
- When comparing the FRP numerical stresses to the analytical predictions given by the existing guidelines to obtain the FRP shear strength contribution, it has been observed that most of the existing guidelines are conservative, assuming stresses between 60% and 75% of the numerical predictions.

The model can be used as a tool to study the effects of different strengthening solutions (configurations, quantities, spacing and thicknesses of FRP) to increase the shear capacity of beams. The computational and modelling simplicity makes it suitable to real scale practical applications.

ACKNOWLEDGEMENTS

The present research has been carried out with the support of the project "Performance-based-design of partially prestressed concrete structures. Proposal of new design methodology, experimental verification and design criteria." (BIA2012-36848) co-financed by the Spanish Ministry of Economics and Competitiveness and the European Funds for Regional Development (FEDER). The Postdoctoral Fellowship conceded by the Government of Catalonia (ref. 2013 PDJ 00022) to the first author is also gratefully acknowledged. The authors acknowledge the support of Albert Alzate, Angel Arteaga, Daniel Cisneros and Ana de Diego from the Instituto de Ciencias de la Construcción Eduardo Torroja of Spain, on the provided data related to their experimental program.

REFERENCES

Alzate, A. (2012). *Análisis de los modelos de comportamiento de vigas de hormigón armado reforzadas a cortante con polímeros armados con fibras (FRP). Validación y calibración experimental*, Ph.D. thesis, Madrid, Universidad Politécnica de Madrid.

American Concrete Institute (ACI) ACI Committee 440. (2008) *Guide for the design and construction of externally bonded FRP systems for strengthening concrete structures, ACI 440.2R-08.*

Cervenka, V. (1985). "Constitutive model for cracked reinforced concrete". *ACI Journal*, 82(6), p. 877-882.

Chen, J. F. and Teng, J. G. (2003) "Shear capacity of FRP-strengthened RC beams: FRP debonding", *Construction and building materials*, 17, 27-41.

CNR (National Research Council) Advisory Committee on technical recommendations for construction. (2004) *Guide for the Design and Construction of Externally Bonded FRP Systems for Strengthening Existing Structures*, CNR-DT200/2004, Rome.

Colajanni, P., La Mendola, L., Recupero, A. (2005). "Shear-flexure interaction of RC elements strengthened with FRP sheets". *Proc. of the 1st Int. Conf. on Concrete Repair, Rehabilitation and Retrofitting*, South Africa, p. 460-462

Comité Europeen de Normalisation. Eurocode 2: design of concrete structures – Part 1.1: General rules and rules for buildings. (2004). CEN EN 1992-1-1:2004.

Concrete Society. (2012). *Design guidance for strengthening concrete structures using fibre composite materials*, London, TR-55.

Federation Internationale du Beton, Task Group 9.3 FRP Reinforcement for Concrete Structures. (2001). *Externally bonded FRP reinforcement for RC structures. Technical report on the design and use of externally bonded fibre reinforced polymer reinforcement (FRP EBR) for reinforced concrete structures*, Fib Bulletin 14, Laussanne.

Ferreira, D., Bairán, J., Marí, A., Faria, R. (2014a). "Nonlinear analysis of RC beams using a hybrid shear-flexural fibre beam model", *Engineering Computations*, 31 (7), p. 1444-1483.

Ferreira, D., Bairán, J., Marí, A. (2014b) "Efficient 1D model for blind assessment of existing bridges: simulation of a full scale loading test and comparison with higher order continuum models", *Structure and Infrastructure Engineering*, DOI:10.1080/15732479.2014.964734

Ferreira, D., Bairán, J., Marí, A. (2013a). "Numerical simulation of shear-strengthened RC beams", *Engineering Structures*, 46, p. 359-374.

Ferreira, D., Oller, E., Marí, A. and Bairán, J. (2013b) "Numerical analysis of shear critical RC beams strengthened in shear with FRP laminates", *J. Comp. Cons.*, 17 (6), 04013016-1-11.

Ferreira., D. (2013) *A model for the nonlinear, time-dependent and strengthening analysis of shear critical frame concrete structures*, Ph.D. Thesis, Barcelona, Universitat Politècnica de Cataluña, Spain.

German Committee for Reinforced Concrete. *DAfStb Heft 595 Erläuterungen und Beispiele zur DAfStb-Richtlinie Verstärken von Betonbauteilen mit geklebter Bewehrung*, Berlin (2013).

448 Khalifa, A. and Nanni, A. (2000) “Improving the shear capacity of existing RC T-section beams using
449 CFRP composites”, *Cement and concrete composites*, 22, 165-174.
450 Khalifa, A. and Nanni, A. (2002) “Rehabilitation of rectangular simply supported RC beams with
451 shear deficiencies using CFRP composites”, *Construction and Building materials*, 16, 135-146.
452 Kotynia, R. (2011) *Shear strengthening of RC beams with polymer composites*. Lodz University of
453 Technology, Lodz, Poland, pp. 310.
454 Kupfer, H., Hilsdorf, H. K. et al. (1969), "Behavior of concrete under biaxial stresses", *ACI J.*, 66(8),
455 656-666.
456 Matthys, S. (2000), "Structural behaviour and design of concrete members strengthened with
457 externally bonded FRP reinforcement", PhD Thesis, Universiteit Gent, Belgium.
458 Mofidi, A., Chaallal, O., Benmokrane, B. and Neale, K. W. (2013) “End-anchorage systems to prevent
459 EB FRP sheets debonding in shear strengthened RC beams”, *Proc. of 11th International*
460 *Symposium on Fiber Reinforced Polymers for Reinfoced Concrete Structures FRPRCS-11*, Ed. J.
461 Barros & J. Sena-Cruz, University of Minho, Guimaraes, 1-5.
462 Mofidi, A. and Chaallal, O. (2013). “Shear strengthening ”, *Proc. of 11th International Symposium on*
463 *Fiber Reinforced Polymers for Reinfoced Concrete Structures FRPRCS-11*, Ed. J. Barros & J.
464 Sena-Cruz, University of Minho, Guimaraes, 1-5.
465 Monti, G., Liotta, M. A. (2007). “Test and design equations for FRP-strengthening in shear”,
466 *Construction and building materials*, 21, 799-809.
467 Oller, E., Cobo, D., and Marí, A. (2009) “Interface behavior in FRP-strengthened beams subjected to
468 transverse loads. Maximum transferred force”, *J. Comp. Cons.*, 13 (1), 35-44.
469 Oller, E. (2005) *Peeling failure in beams externally strengthened by plate bonding. A design proposal*,
470 Ph.D. thesis, Universidad Politécnica de Cataluña, Barcelona, Spain.
471 Pellegrino, C., and Modena, C. (2006) “Fiber-reinforced polymer shear strengthening of reinforced
472 concrete beams: experimental study and analytical modeling”, *ACI Structural Journal*, 103 (5),
473 720-728.

Pellegrino, C., and Vasic, M. (2013) “Assessment of design procedures for the use of externally bonded FRP composites in shear strengthening of reinforced concrete beams”, *Composites: part B*, 45, 727-741.

Sas, G., Täljsten, B., Barros, J., Lima, J., Carolin, A. (2009) “Are available models reliable for predicting the FRP contribution to the shear resistance of RC beams?”, *Journal of Composites for Construction*, 13(6), p. 514–34.

Spoelstra, M. R. and Monti, G. (1999). “FRP-confined concrete model”, *Journal of Composites for Construction*, 3(3), p. 143-150.

Vecchio, F. J. and Collins, M. P. (1986), "The modified compession-fiel theory for reinforced concrete elements subjected to shear", *ACI J.*, 83(2), 1357-1417.

Table 1. Material properties for concrete, bond and FRP

Tests	Concrete properties				Bond properties		FRP strengthening properties				
	f_{cm} (MPa)	E_c (MPa)	f_{ctm} (MPa)	$\varepsilon_{c,u}$	G_f (MPa.mm)	τ_{LM} (MPa)	t_f (mm)	ρ_{FRP}	E_{FRP} (MPa)	$\varepsilon_{FRP,u}$	$f_{FRP,u}$ (MPa)
U90S5-a	36.95	32560	3.33	0.0035	0.717	2.24	0.293	0.0088	240000	0.0150	4000
U90S5-b	28.01	29970	2.77	0.0035	0.596	1.85	0.293	0.0088	240000	0.0150	4000
U90S3-a	20.50	27290	2.25	0.0035	0.484	1.49	0.176	0.0053	240000	0.0155	3800
U90S3-b	22.58	28090	2.40	0.0035	0.516	1.59	0.176	0.0053	240000	0.0155	3800
U90S3-c	28.01	29970	2.77	0.0035	0.596	1.85	0.176	0.0053	240000	0.0155	3800
W90S5	49.90	34976	3.90	0.0180	No debonding check		0.293	0.0088	240000	0.0150	4000
W90S3-ab	37.00	32575	3.33	0.0130	No debonding check		0.176	0.0053	240000	0.0155	3800
W90S3-b	37.00	32575	3.33	0.0130	No debonding check		0.176	0.0053	240000	0.0155	3800
BS4	38.40	34100	5.72	0.0035	2.557	4.28	0.110	1.1	233000	0.01502	3500
BS5	36.00	33746	3.27	0.0035	2.453	4.10	0.110	0.00014	233000	0.01502	3500
SO-3-2	27.50	25000	2.73	0.0035	1.088	2.72	0.165	0.0009	228000	0.01662	3790
SO-3-3	27.50	25000	2.73	0.0035	0.959	2.55	0.165	0.0013	228000	0.01662	3790
SO-3-4	27.50	25000	2.73	0.0035	1.296	2.97	0.165	0.0022	228000	0.01662	3790
SO-4-2	27.50	25000	2.73	0.0035	1.088	2.72	0.165	0.0009	228000	0.01662	3790
SO-4-3	27.50	25000	2.73	0.0035	1.296	2.97	0.165	0.0022	228000	0.01662	3790

Table 2. Summary of experimental and numerical results at failure

Tests	Experimental data			Numerical results							
				Failure				Debond failure related results			
	P_u (kN)	V_u (kN)	Failure mode	P_u (kN)	V_u (kN)	Failure mode	$P_{u,num}$ / $P_{u,exp}$	$V_{u,deb}$ (kN)	$V_{u,deb}$ / V_u	σ_z^{FRP} (MPa)	$\sigma_{max,deb}$ (MPa)
U90S5-a	341	247	DS	341	241	PS	1.00	240	0.99	1109	1084
U90S5-b	326	236	DS	315	223	PS	0.97	222	0.99	991	988
U90S3-a	285	207	DS	263	186	PS	0.92	186	1.00	1151	1149
U90S3-c	320	232	DS	311	219	PS	0.97	219	1.00	1332	1275
W90S5	383	276	BS	402	284	BS	1.05	NP	-	-	-
W90S3-ab	432	311	BS	408	289	BS	0.94	NP	-	-	-
W90S3-b	394	284	BS	408	289	BS	1.04	NP	-	-	-
BS4	504	256	B	498	249	B	0.99	NP	-	-	-
BS5	340	174	DS	355	178	DS	1.04	178	1.00	2348	3223
SO-3-2	262	131	DS	260	130	DS	0.99	130	1.00	1710	1710
SO-3-3	266	133	DS	230	115	S-ND	0.86	-	-	-	-
SO-3-4	289	144.5	DS	380	190	S-ND	1.31	-	-	-	-
SO-4-2	255	127.5	DS	270	135	DS	1.06	135	1.00	1710	1710
SO-4-3	310	155	BS	281	140.5	BS	0.91	-	-	-	-

DS= Debonding FRP - Shear

BS=bending-shear

ND= No Debonding

B=bending

S=shear

Table 3. FRP stresses at debonding. Comparison between numerical and analytical predictions.

Test	Numerical	Analytical				
	σ_z^{FRP} (MPa)	Fib bulletin 14 (2001)	ACI 440.2R-08 (2008)	CNR-DT200/2004 (2004)	TR-55 (2012)	DafStb Heft 595 (2013)
		$\sigma_{max,deb}$ (MPa)	$\sigma_{max,deb}$ (MPa)	$\sigma_{max,deb}$ (MPa)	$\sigma_{max,deb}$ (MPa)	$\sigma_{max,deb}$ (MPa)
U90S5-a	1109	1103 (1.01)	771 (1.44)	660 (1.68)	826 (1.34)	817 (1.36)
U90S5-b	991	994 (1.00)	641 (1.55)	582 (1.70)	753 (1.32)	728 (1.36)
U90S3-a	1151	1221 (0.94)	681 (1.69)	696 (1.65)	904 (1.27)	852 (1.35)
U90S3-c	1332	1372 (0.97)	838 (1.59)	801 (1.66)	960 (1.39)	970 (137)
BS5	2348	3411 (0.69)	932 (2.52)	1216 (1.93)	932 (2.52)	1295 (1.81)
SO-3-2	1710	1381 (1.24)	912 (1.88)	925 (1.85)	912 (1.88)	1044 (1.64)
SO-3-3	-	1101 (-)	912 (-)	906 (-)	912 (-)	1044 (-)
SO-3-4	-	827 (-)	912 (-)	838 (-)	912 (-)	-
SO-4-2	1710	1381 (1.24)	912 (1.88)	925 (1.85)	912 (1.88)	1044 (1.64)
SO-4-3	-	827 (-)	912 (-)	838 (-)	912 (-)	-

*in brackets numerical to analytical ratios

Figure 01

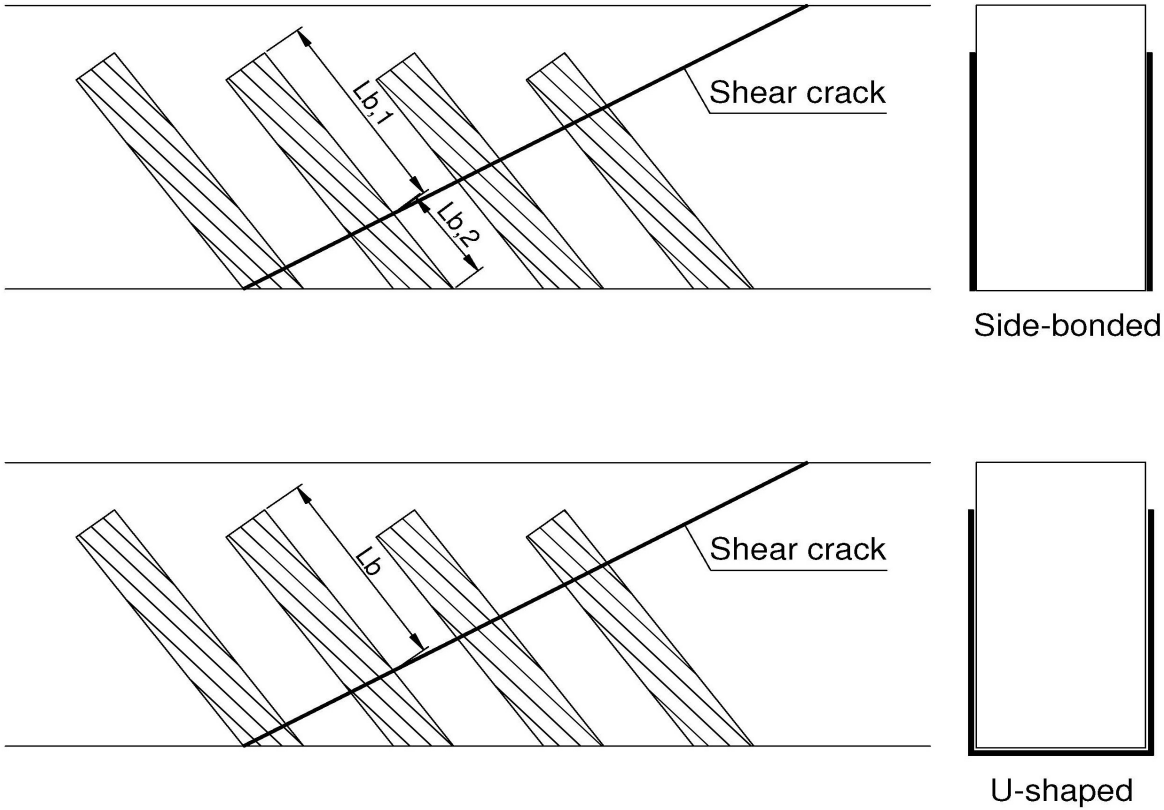

Figure 02

Click here to download Figure Figure 02.pdf

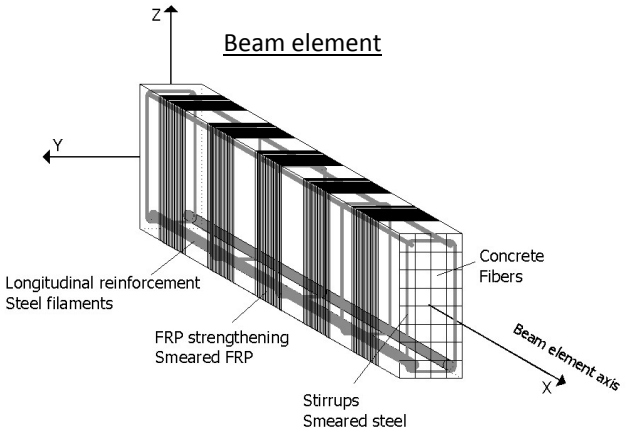

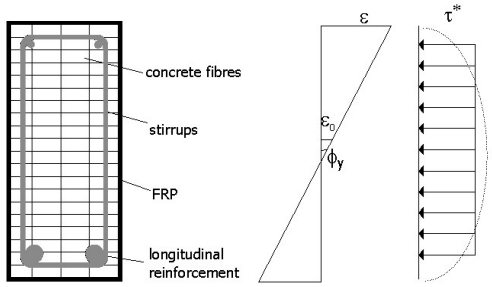

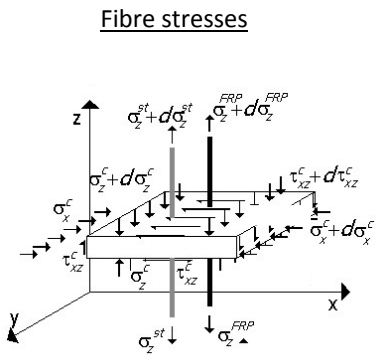

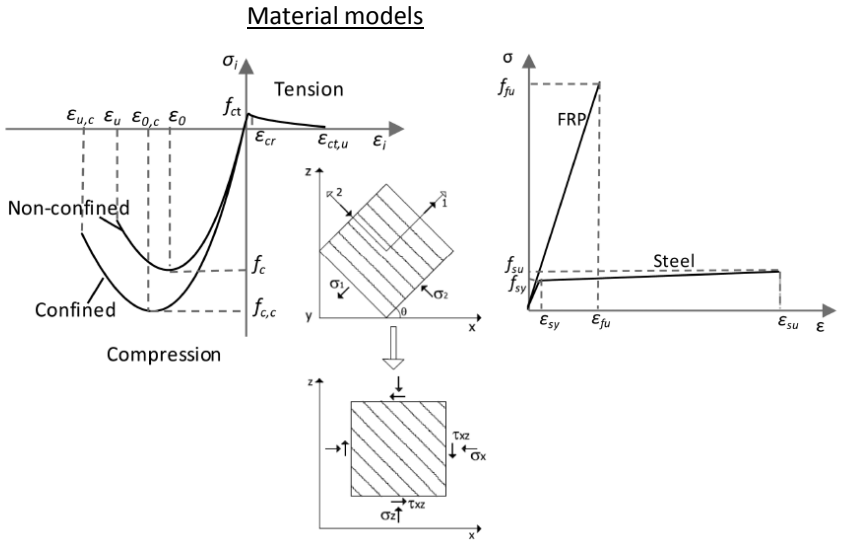

Figure 03

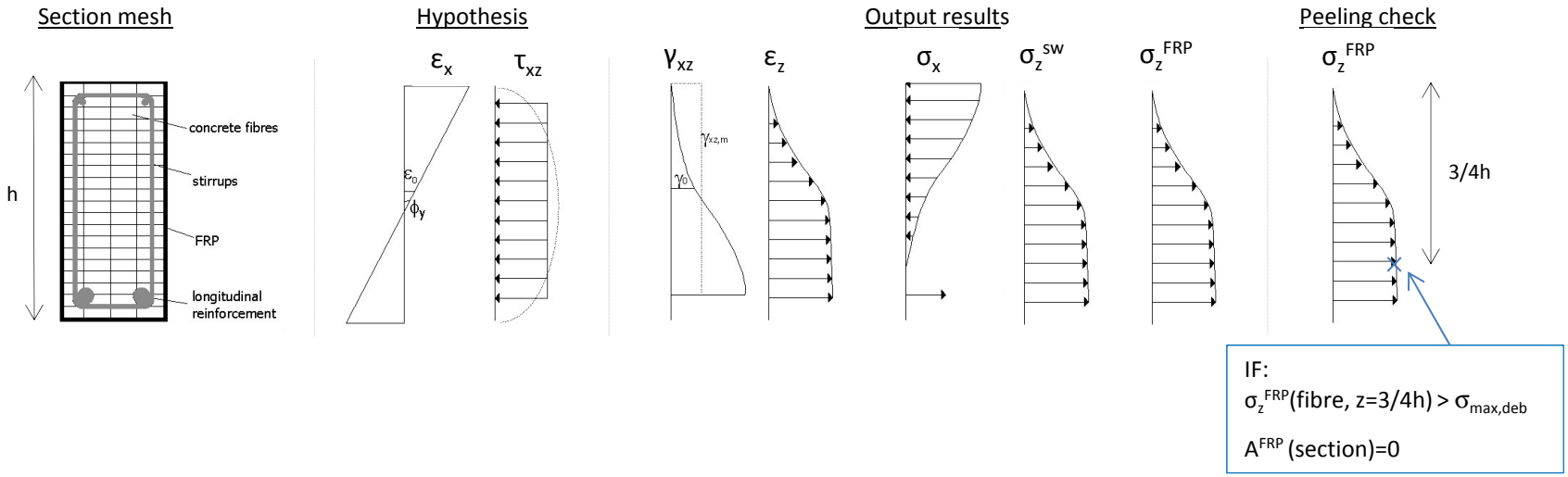

Figure 04

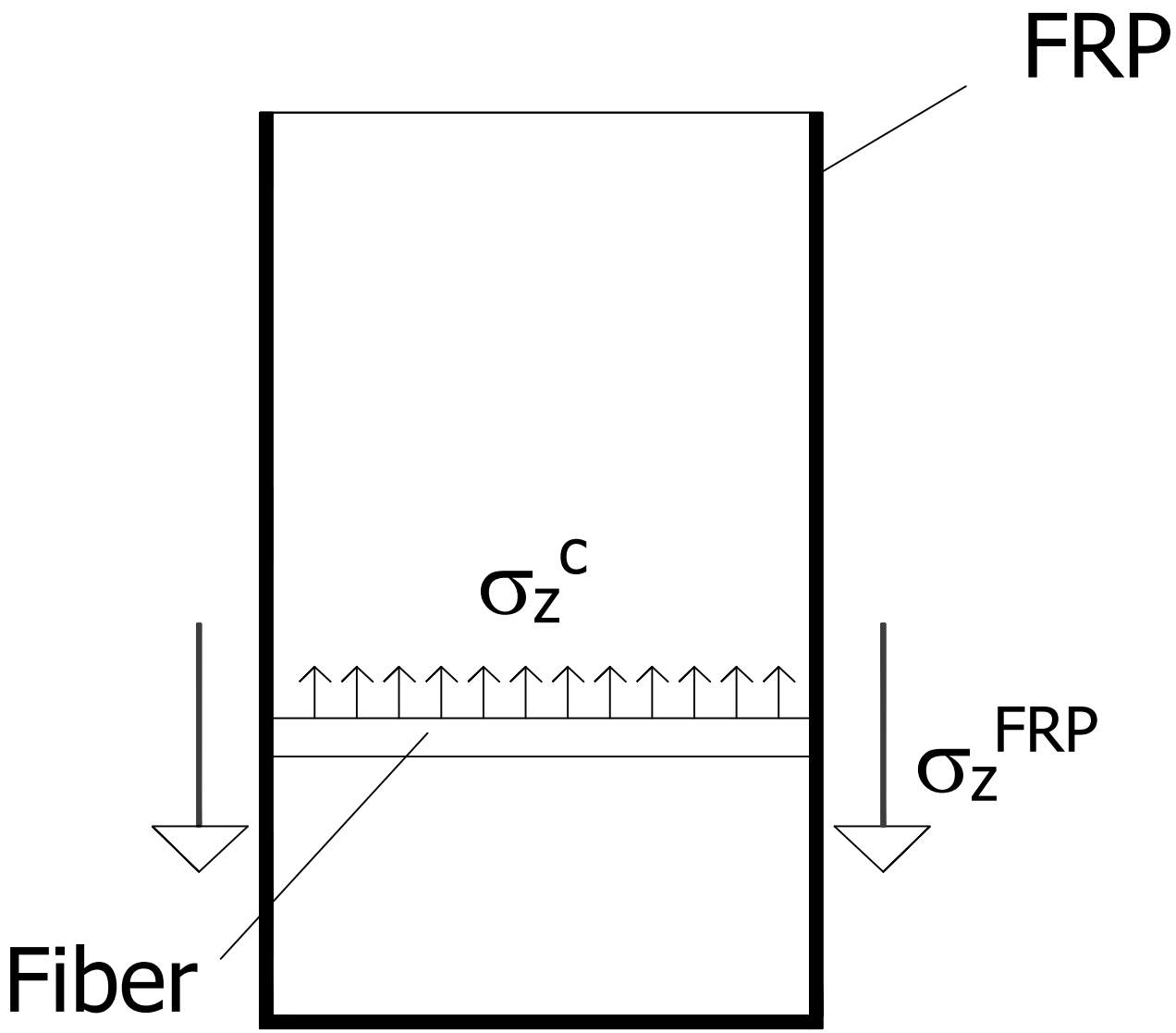

W90 (S530 & S300)

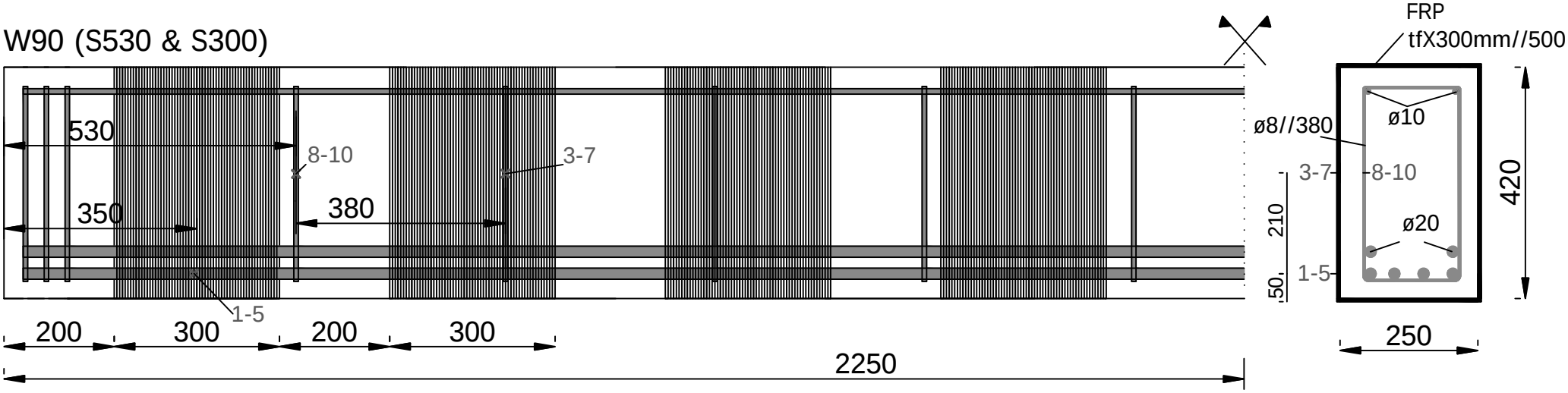

U90 (S530 & S300

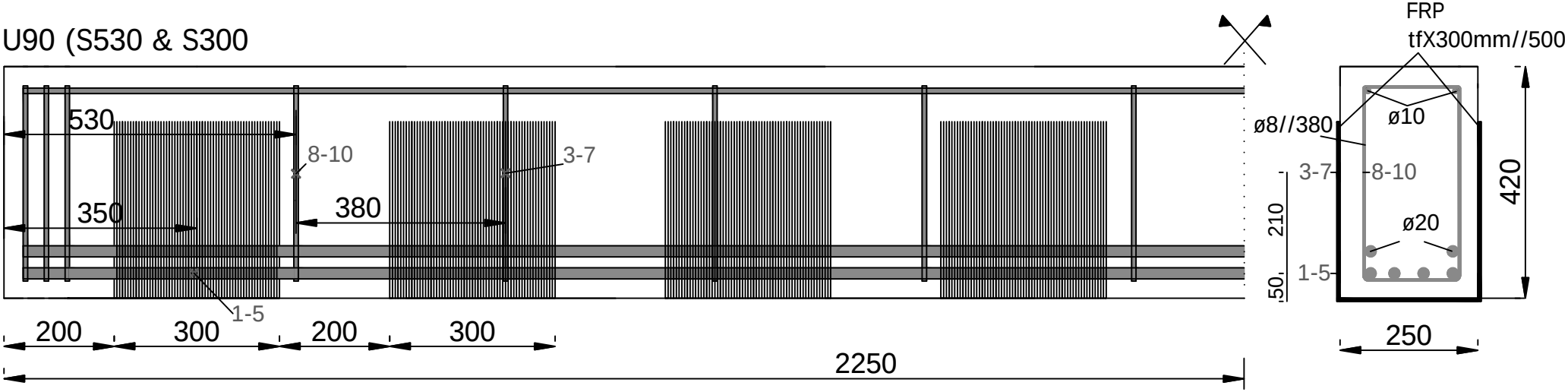

Figure 06

Click here to download Figure Figure 06.pdf

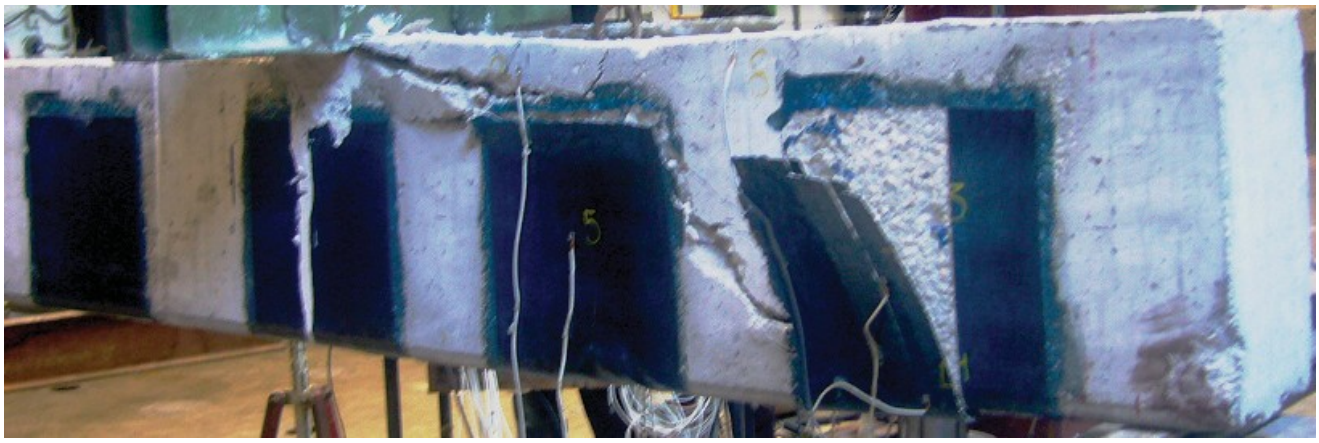

Figure 07

Click here to download Figure Figure 07.pdf

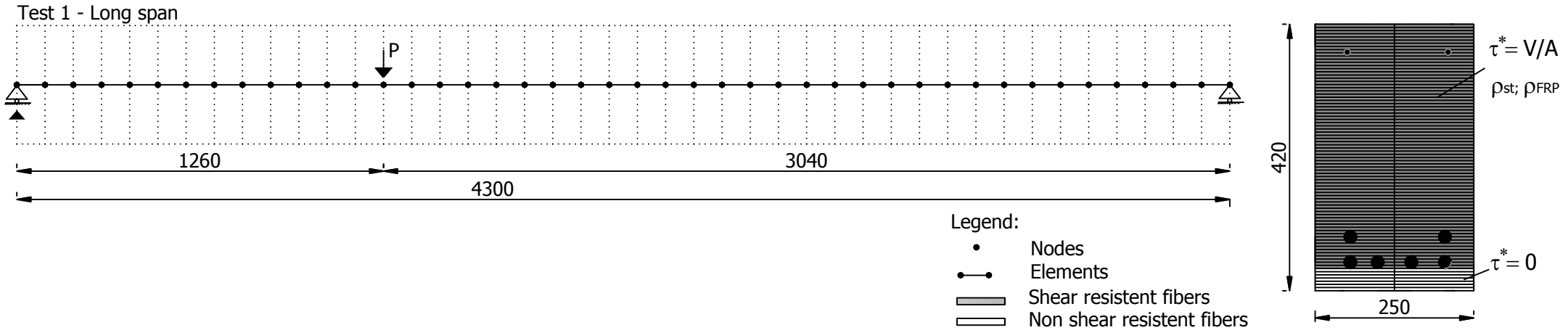

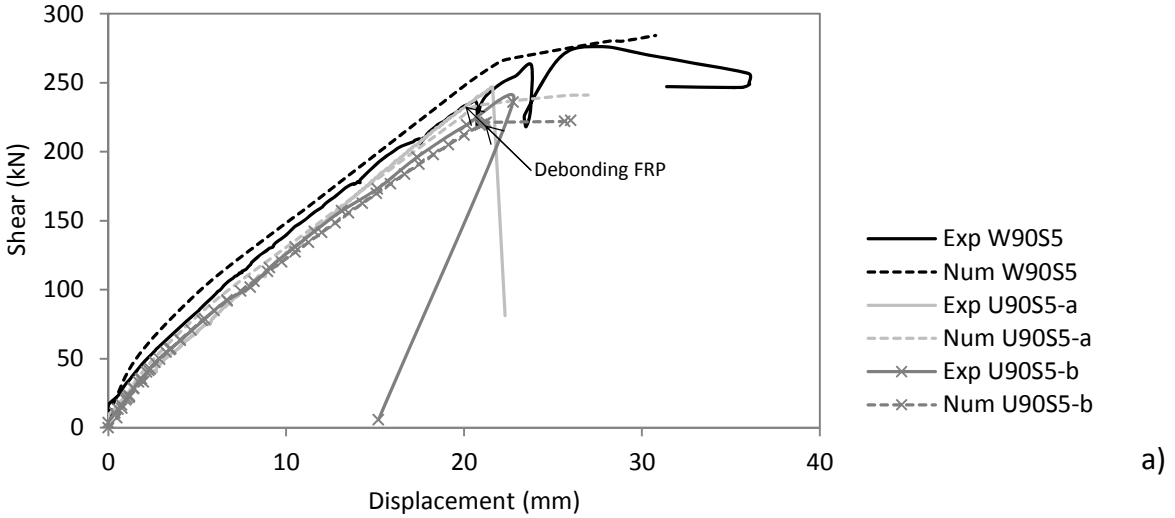
300
250
200
150
100
50
0
Shear (kN)
0
10
20
30
40
Displacement (mm)
Debonding FRP
Exp W90S5
Num W90S5
Exp U90S5-a
Num U90S5-a
Exp U90S5-b
Num U90S5-b

a)

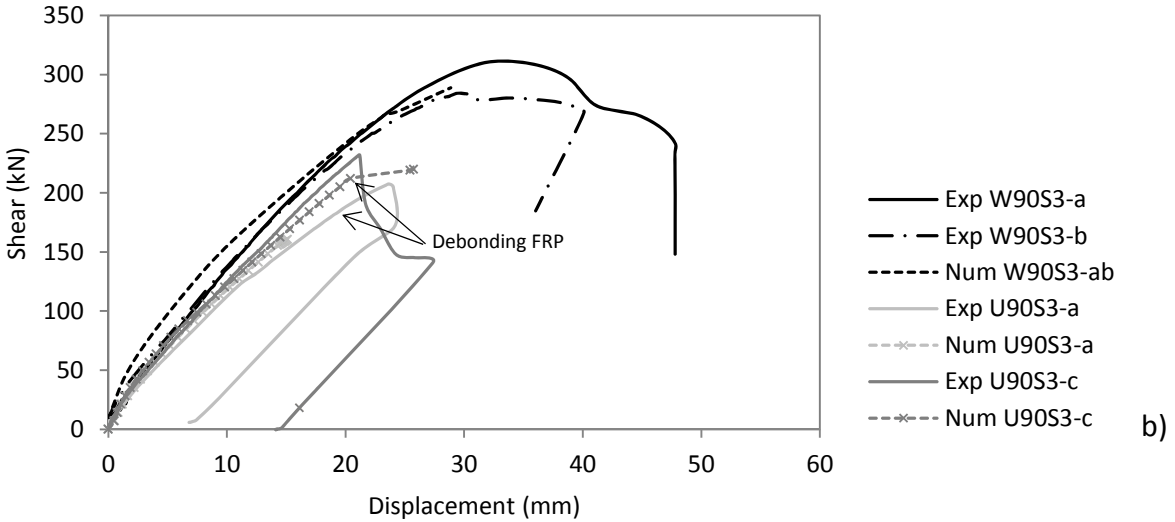
350
300
250
200
150
100
50
0
Shear (kN)
0
10
20
30
40
50
60
Displacement (mm)
Debonding FRP
Exp W90S3-a
Exp W90S3-b
Num W90S3-ab
Exp U90S3-a
Num U90S3-a
Exp U90S3-c
Num U90S3-c

b)

Figure 09

Click here to download Figure Figure 09.pdf

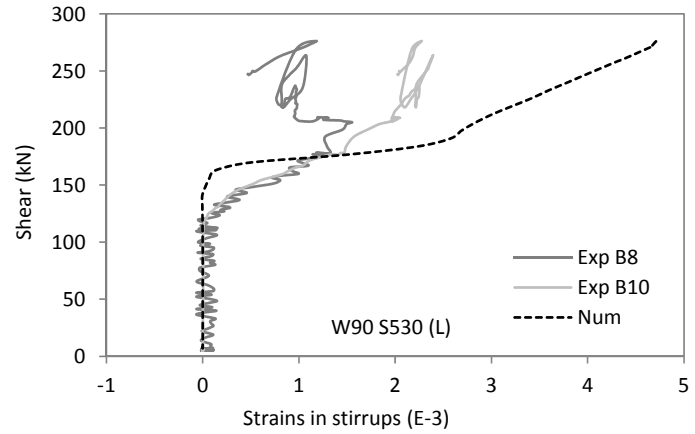

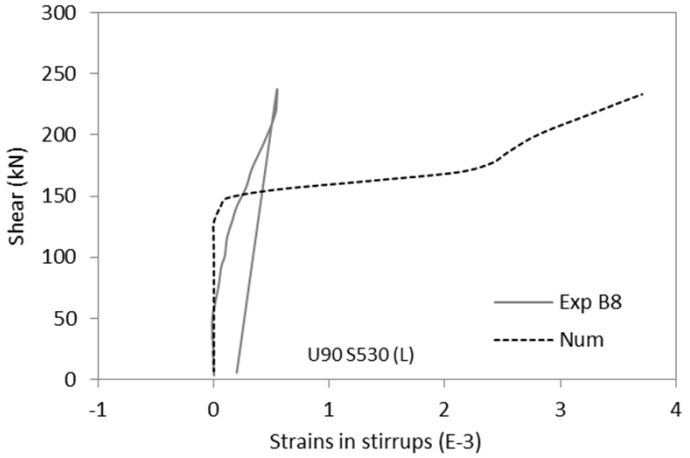

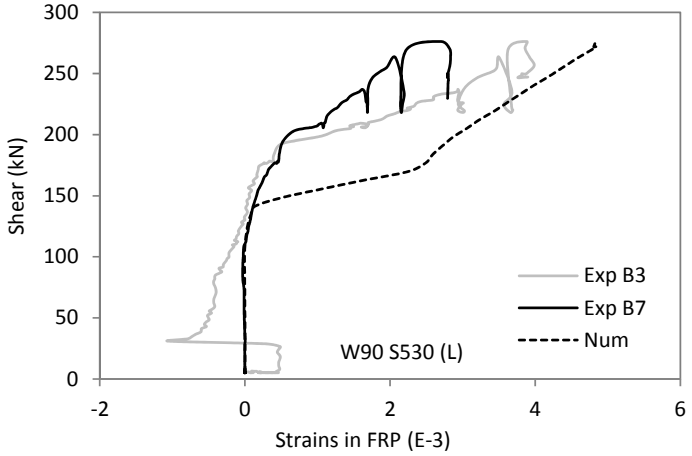

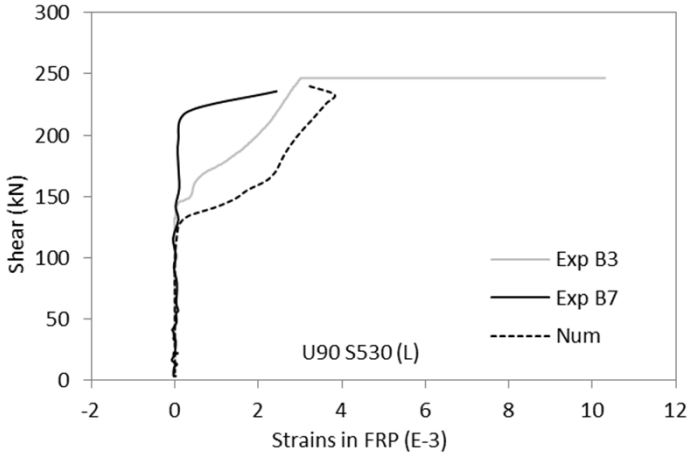

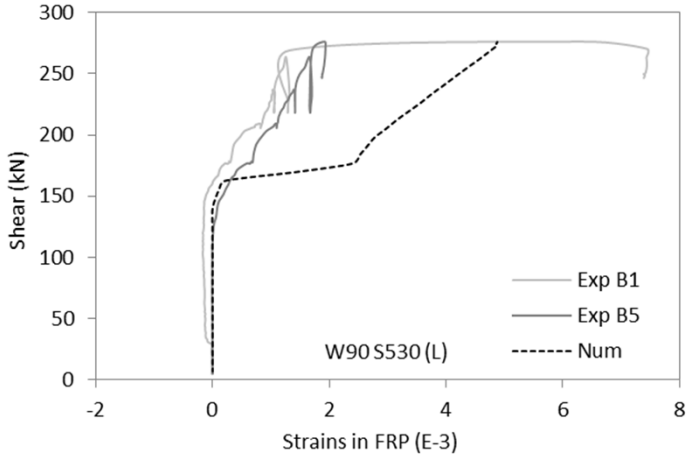

a)

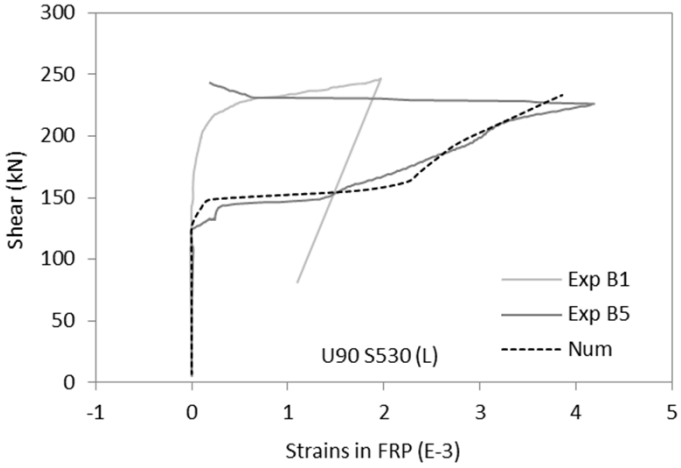

b)

Figure 10

Click here to download Figure Figure 10.pdf

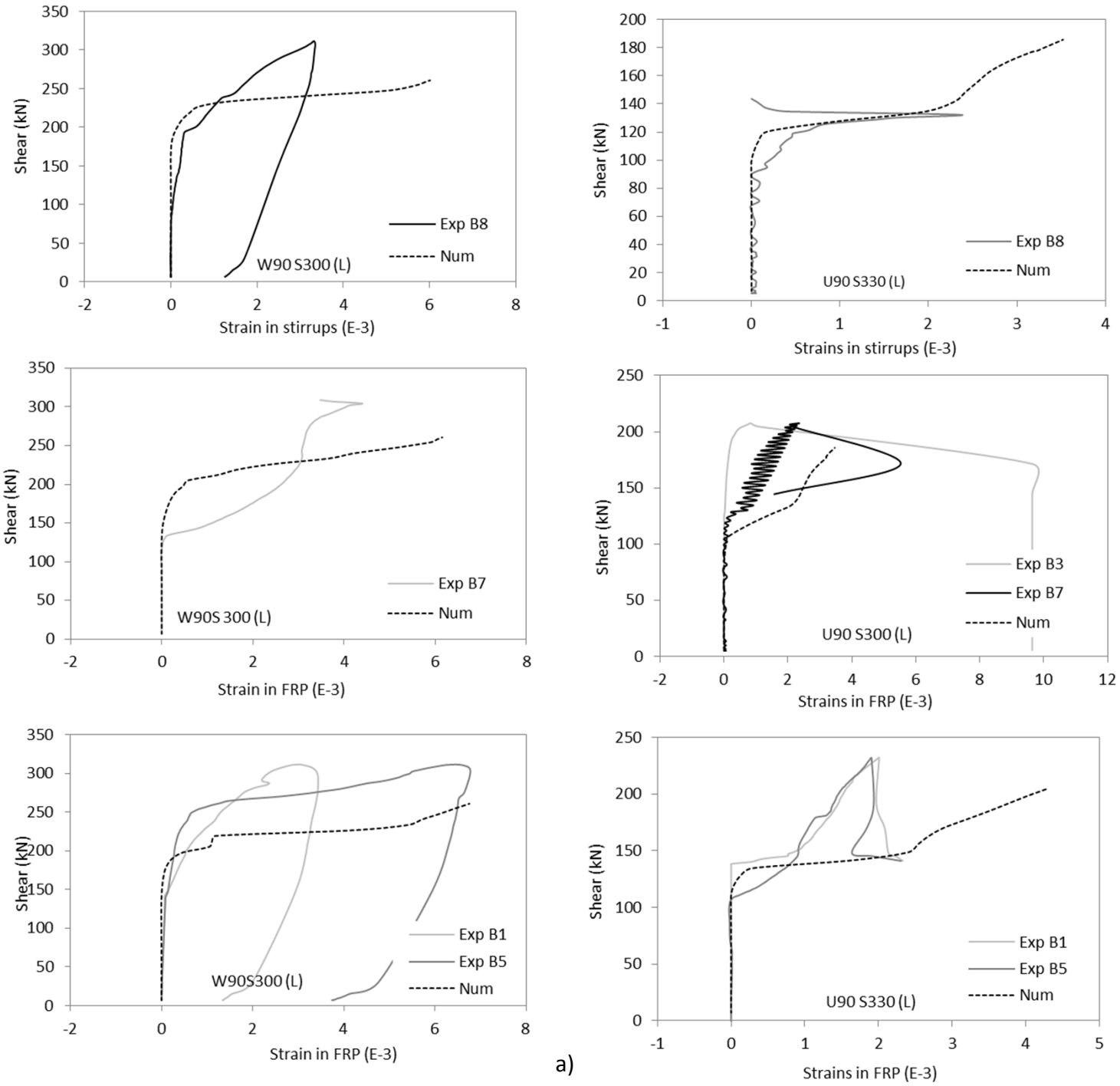

Figure 11

Click here to download Figure Figure 11.pdf

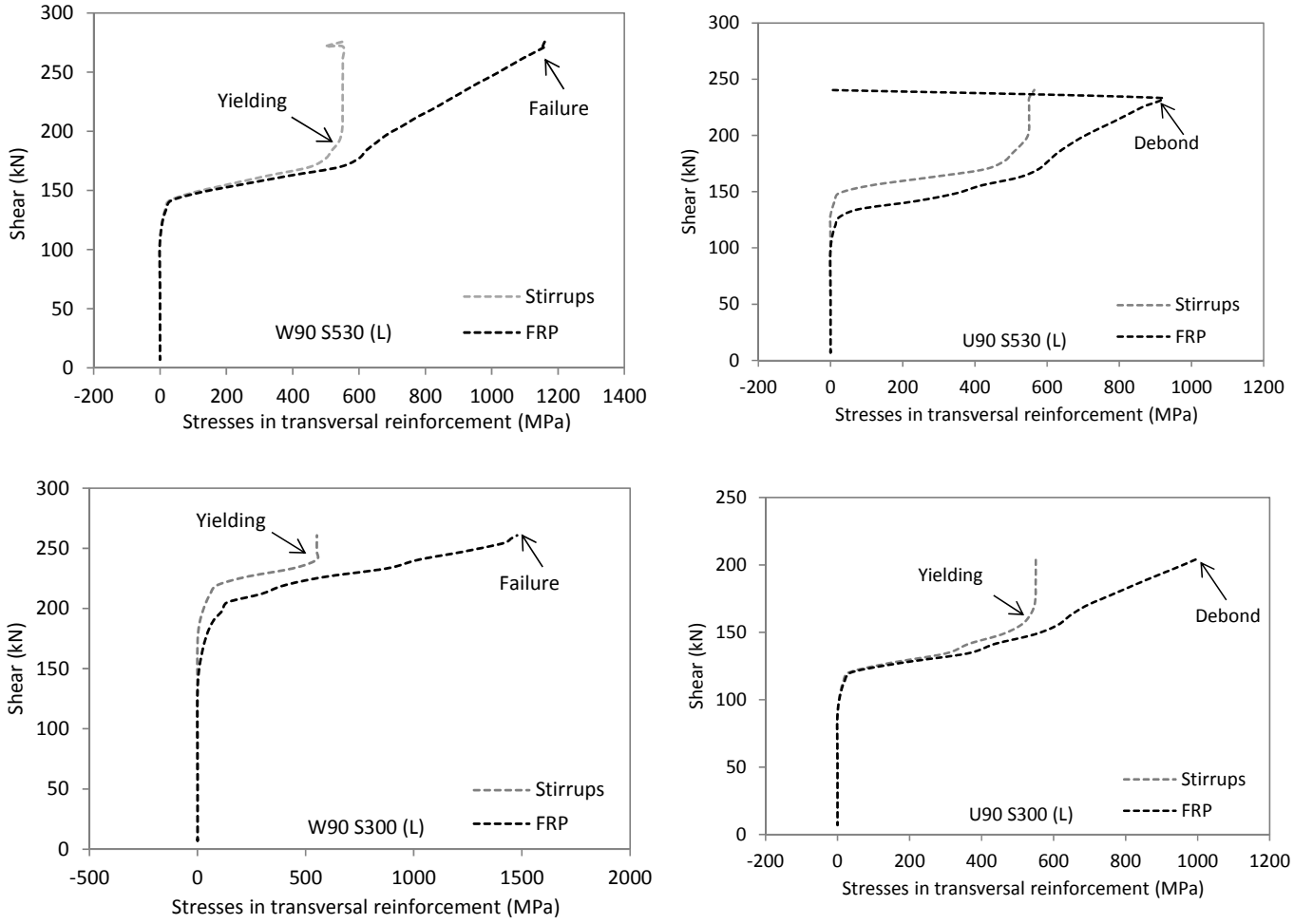

Figure 12

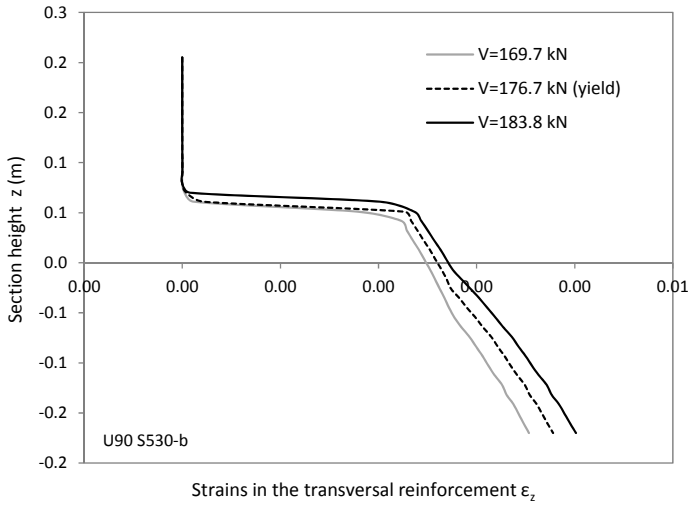

a)

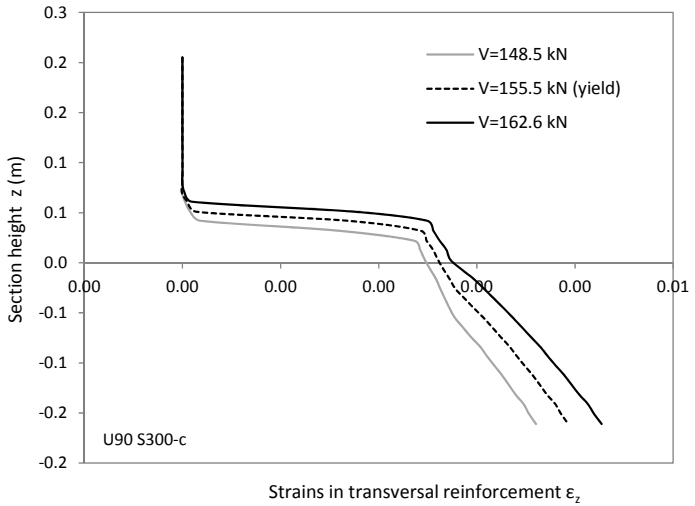

b)

Figure 13

Click here to download Figure Figure 13.pdf

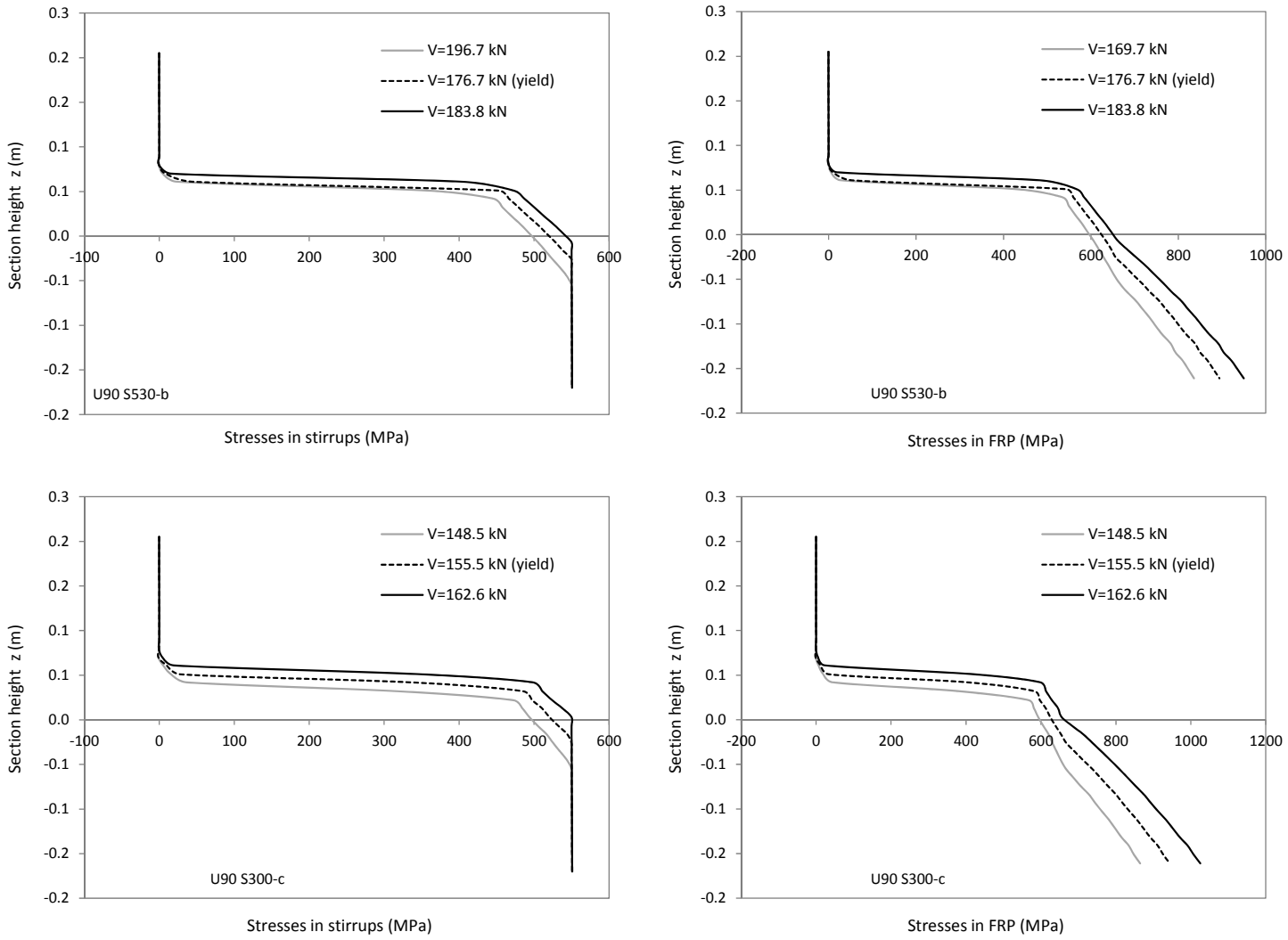

a) b)

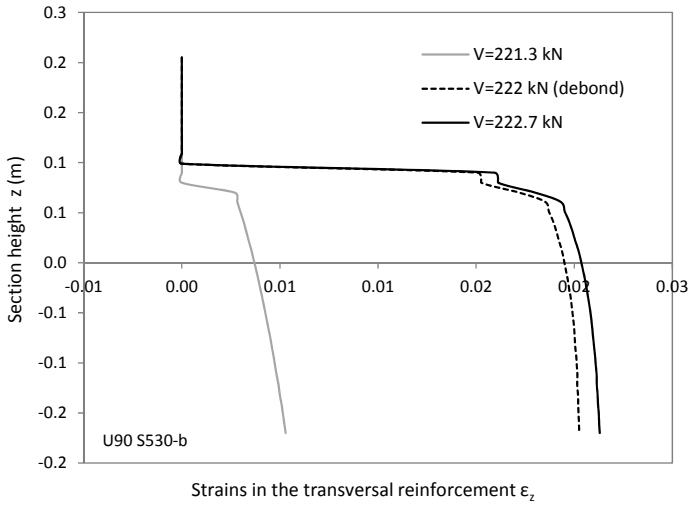
V=221.3 kN
V=222 kN (debond)
V=222.7 kN
U90 S530-b
Section height z (m)
Strains in the transversal reinforcement ε_z

a)

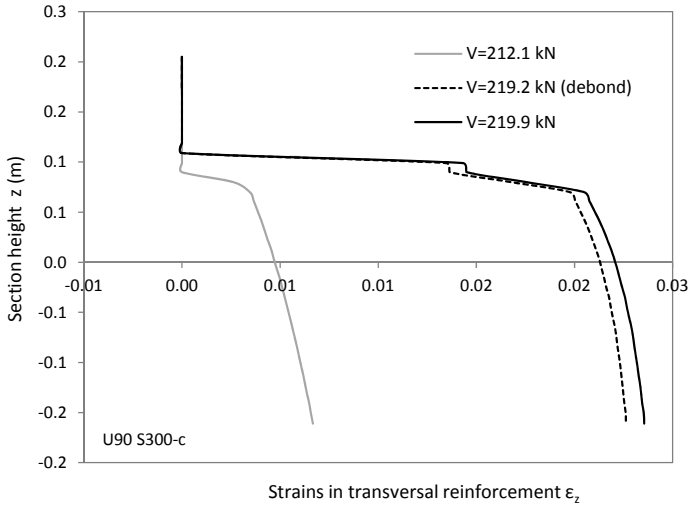
V=212.1 kN
V=219.2 kN (debond)
V=219.9 kN
U90 S300-c
Section height z (m)
Strains in transversal reinforcement ε_z

b)

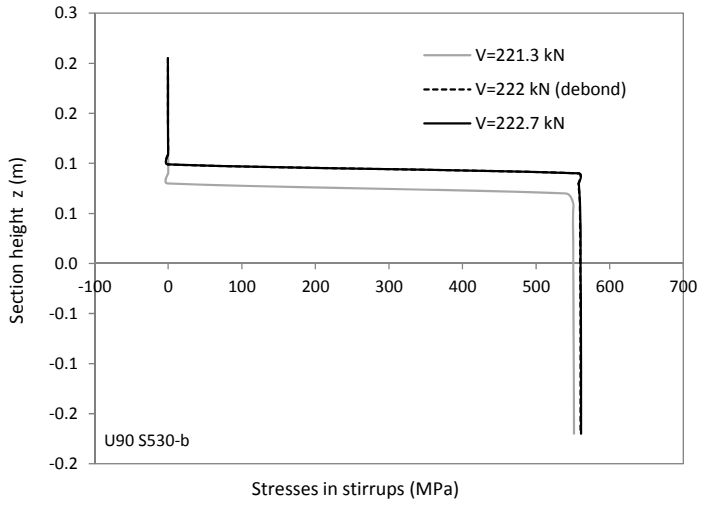
V=221.3 kN
V=222 kN (debond)
V=222.7 kN
Section height z (m)
Stresses in stirrups (MPa)
U90 S530-b

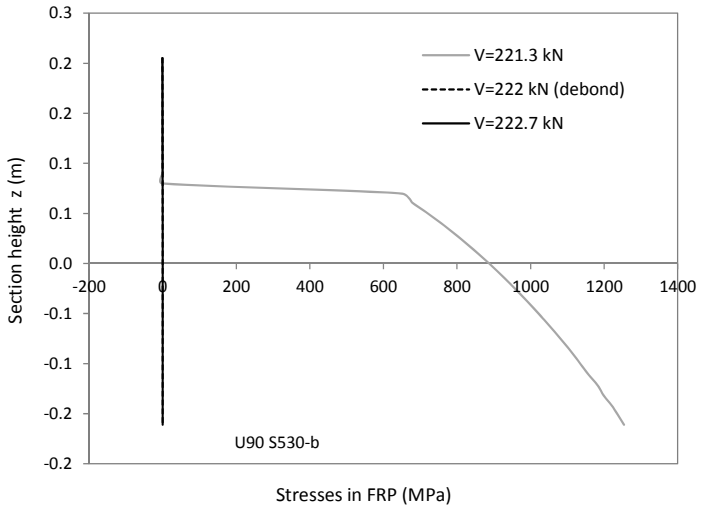
V=221.3 kN
V=222 kN (debond)
V=222.7 kN
Section height z (m)
Stresses in FRP (MPa)
U90 S530-b

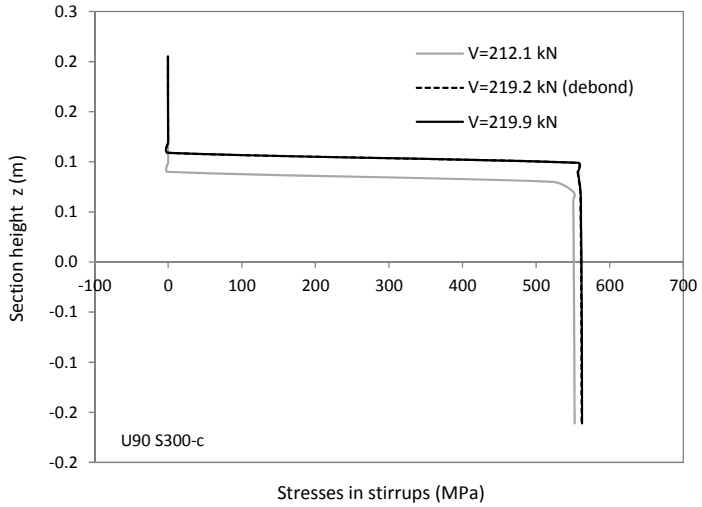
V=212.1 kN
V=219.2 kN (debond)
V=219.9 kN
Section height z (m)
Stresses in stirrups (MPa)
U90 S300-c

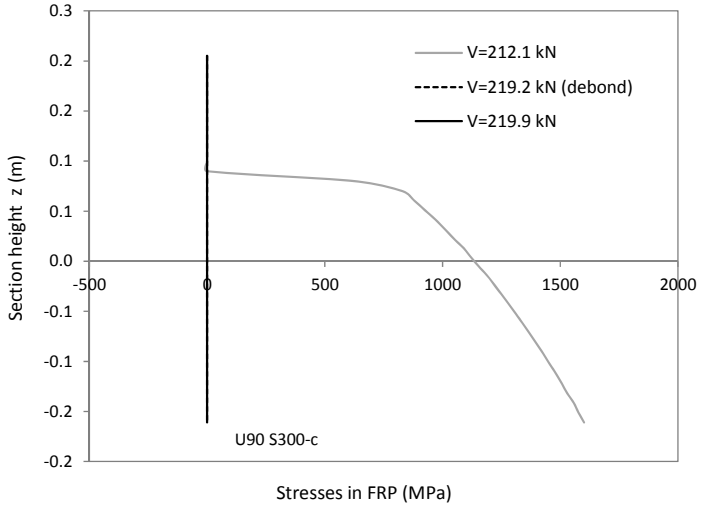
V=212.1 kN
V=219.2 kN (debond)
V=219.9 kN
Section height z (m)
Stresses in FRP (MPa)
U90 S300-c

a)

b)

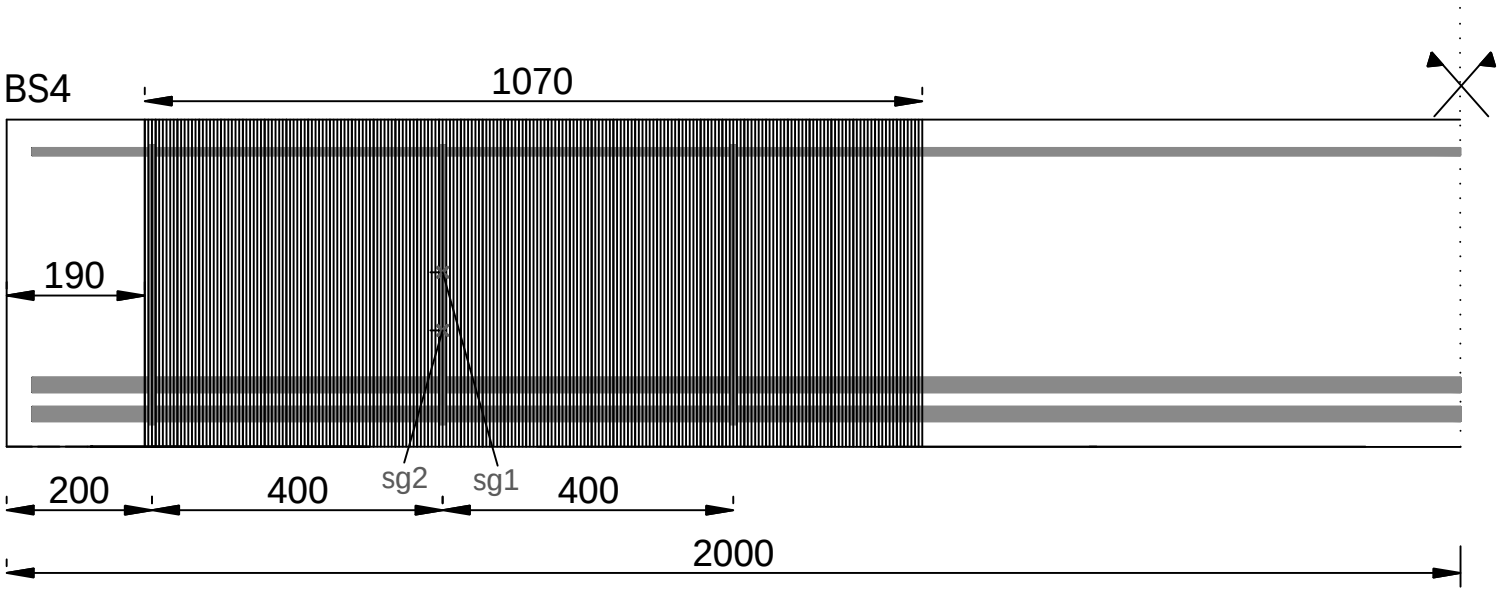
BS4
1070
190
sg2
sg1
200
400
400
2000

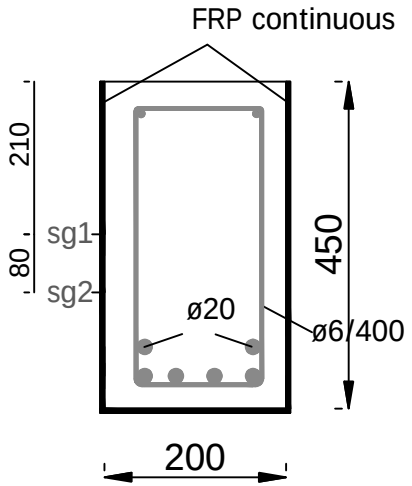
FRP continuous
210
80
sg1
sg2
ø20
ø6/400
450
200

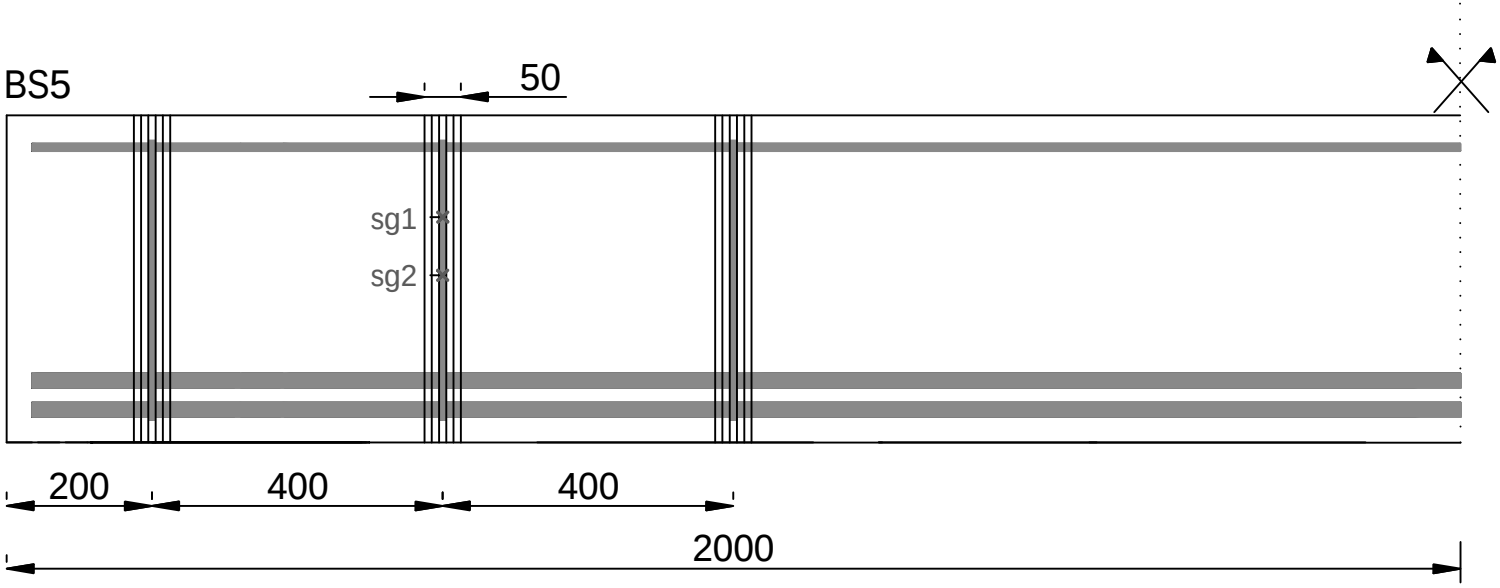
BS5
50
sg1
sg2
200
400
400
2000

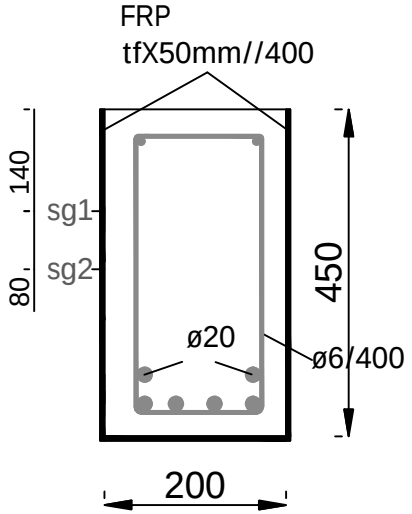
FRP
tfX50mm//400
140
80
sg1
sg2
ø20
ø6/400
450
200

Figure 17

Click here to download Figure Figure 17.pdf

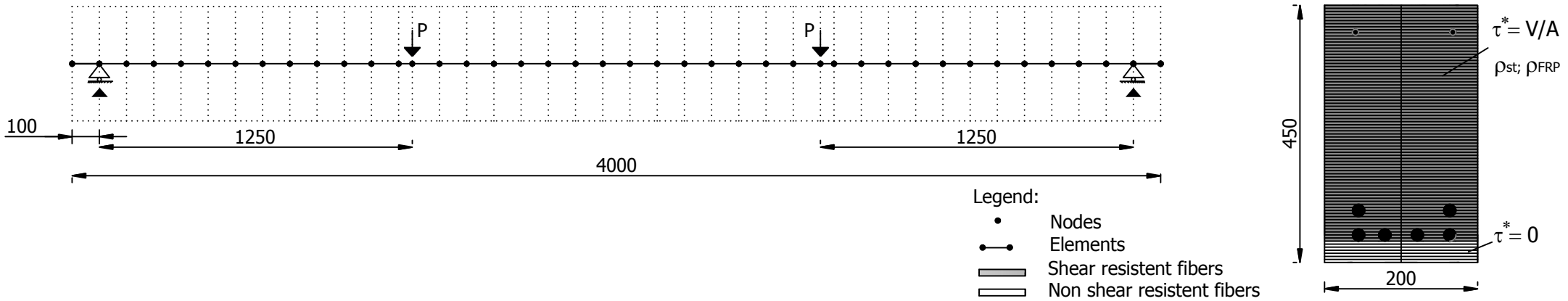

Figure 18

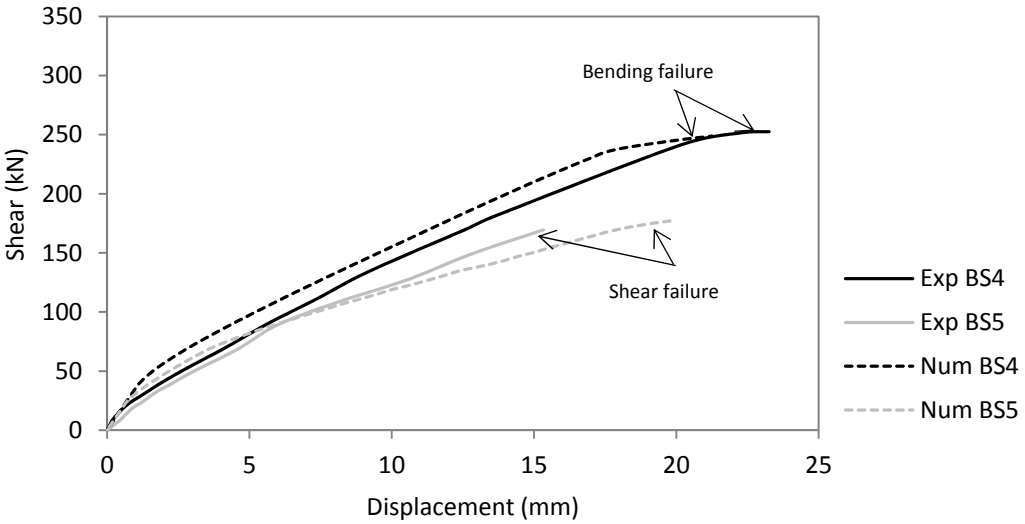

Figure 19a

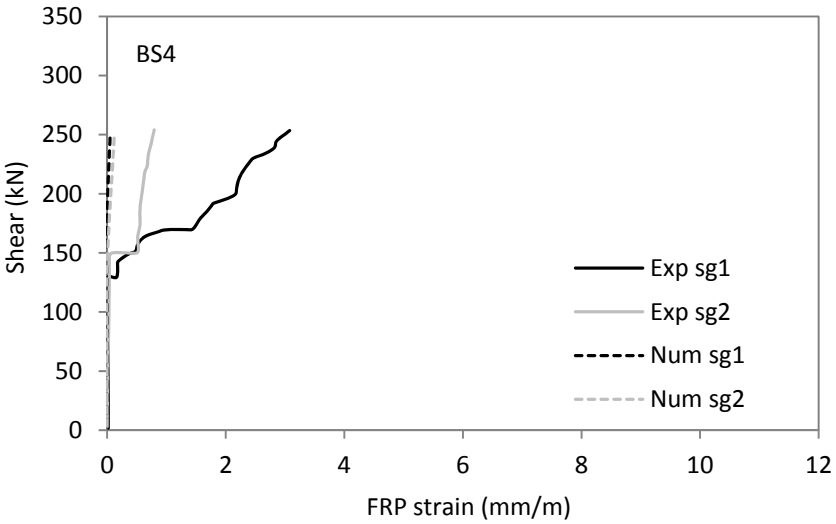

Figure 19b

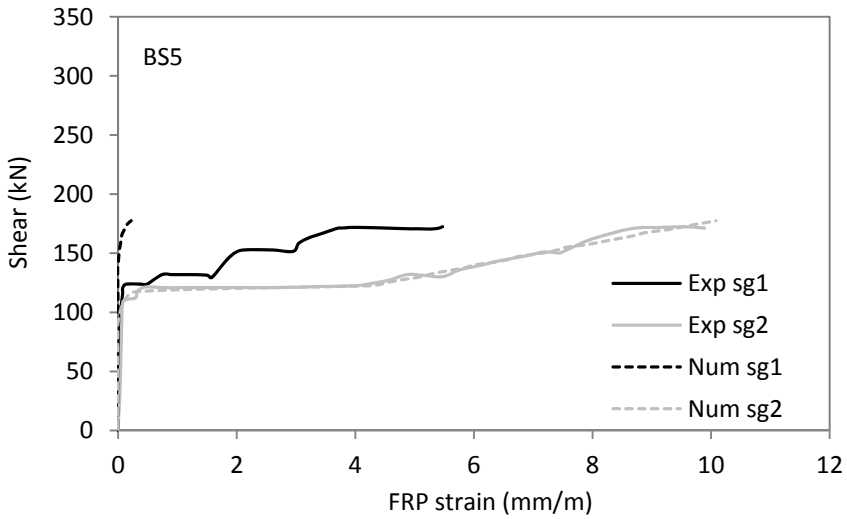

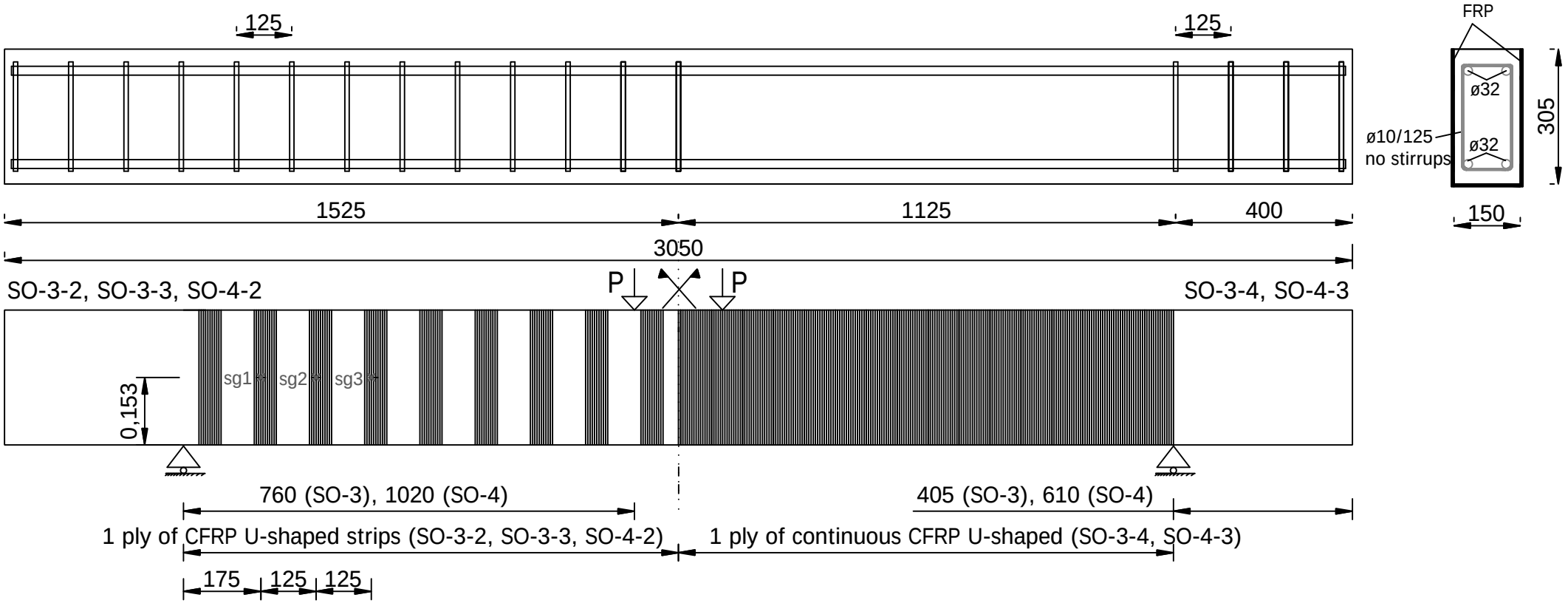
125
125
FRP
ø32
ø32
ø10/125
no stirrups
305
150
1525
1125
400
3050
SO-3-2, SO-3-3, SO-4-2
P
P
SO-3-4, SO-4-3
sg1
sg2
sg3
0,153
760 (SO-3), 1020 (SO-4)
405 (SO-3), 610 (SO-4)
1 ply of CFRP U-shaped strips (SO-3-2, SO-3-3, SO-4-2)
1 ply of continuous CFRP U-shaped (SO-3-4, SO-4-3)
175
125
125

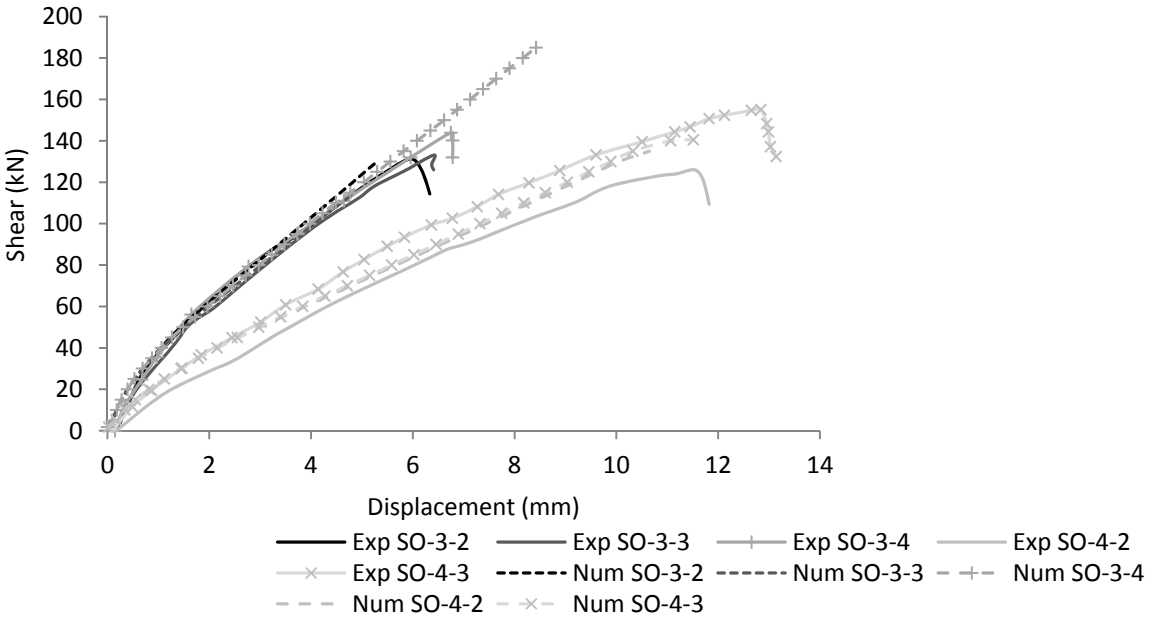
Shear (kN)
200
180
160
140
120
100
80
60
40
20
0
0
2
4
6
8
10
12
14
Displacement (mm)
Exp SO-3-2
Exp SO-3-3
Exp SO-3-4
Exp SO-4-2
Exp SO-4-3
Num SO-3-2
Num SO-3-3
Num SO-3-4
Num SO-4-2
Num SO-4-3

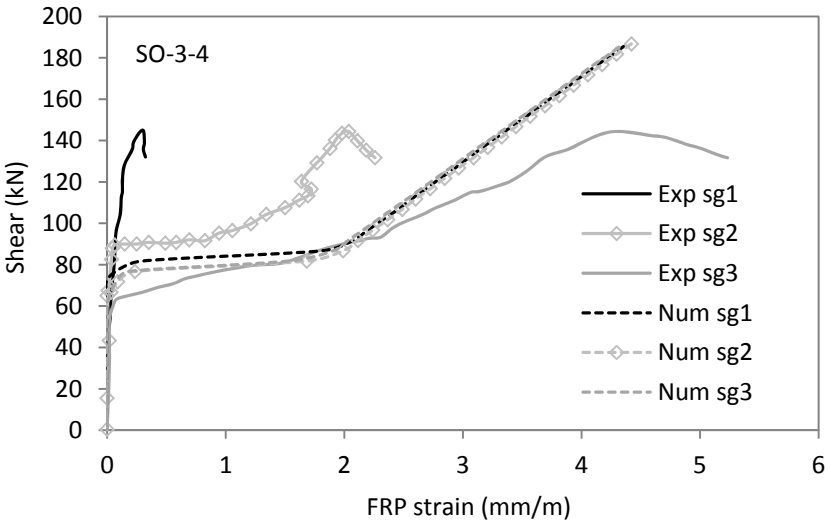
SO-3-4
Shear (kN)
FRP strain (mm/m)
200
180
160
140
120
100
80
60
40
20
0
0
1
2
3
4
5
6
Exp sg1
Exp sg2
Exp sg3
Num sg1
Num sg2
Num sg3

Figure 23

Click here to download Figure Figure 23.pdf

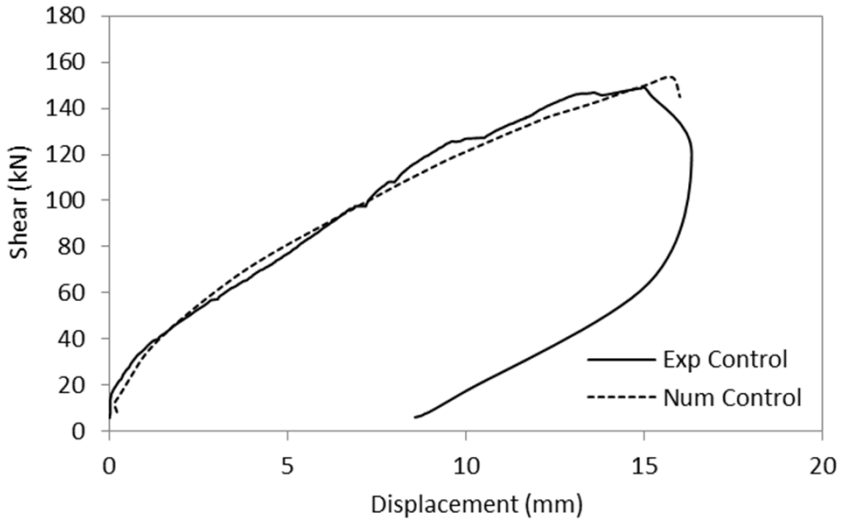

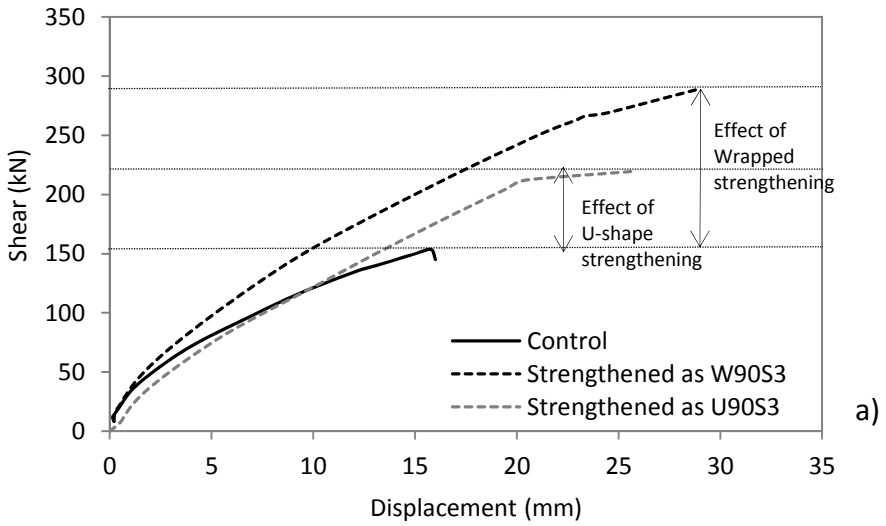
350
300
250
200
150
100
50
0
Shear (kN)
0
5
10
15
20
25
30
35
Displacement (mm)
Effect of
Wrapped
strengthening
Effect of
U-shape
strengthening
Control
Strengthened as W90S3
Strengthened as U90S3

a)

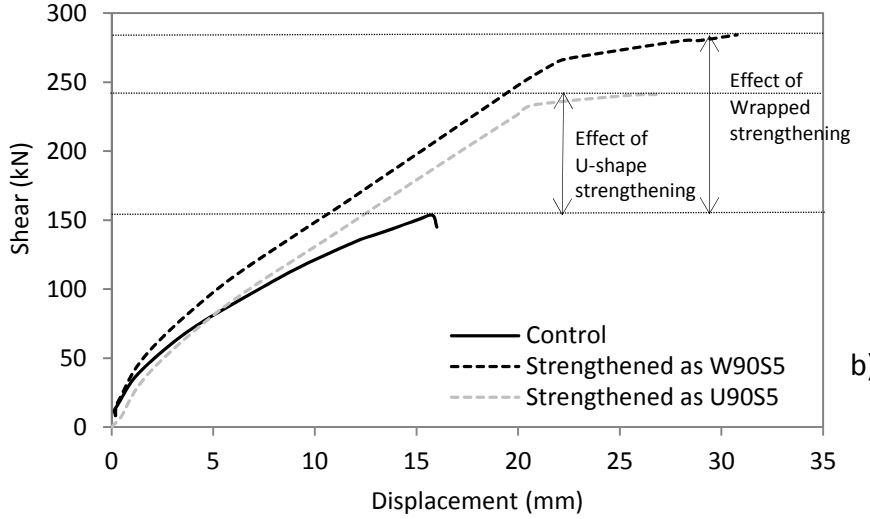
300
250
200
150
100
50
0
Shear (kN)
0
5
10
15
20
25
30
35
Displacement (mm)
Effect of
Wrapped
strengthening
Effect of
U-shape
strengthening
Control
Strengthened as W90S5
Strengthened as U90S5

b)

Fig. 23. Response of the shear critical RC beam (Control especimen)

Fig. 24. Gain of shear resistance with FRP strengthening with different solutions: a) FRP S530 and b) FRP S300